file

I.O.S.

THE USE OF DEPTH-AVERAGED CURRENTS TO
ESTIMATE BED SHEAR STRESS
as applied to a numerical model of
the Sizewell-Dunwich Bank Area
by
R L SOULSBY

NATURAL ENVIRONMENT RESEARCH COUNCIL

**INSTITUTE OF
OCEANOGRAPHIC
SCIENCES**

THE USE OF DEPTH-AVERAGED CURRENTS TO
ESTIMATE BED SHEAR STRESS
as applied to a numerical model of
the Sizewell-Dunwich Bank Area
by
R L SOULSBY

This document should not be cited in any paper or report except as
'personal communication', and is for the use of the recipient only.

CONTENTS

THE USE OF DEPTH-AVERAGED CURRENTS TO ESTIMATE BED SHEAR STRESS

as applied to a numerical model of the Sizewell-Dunwich Bank area

Specification of the Problem

The problem tackled in this report has arisen in connection with the development
by IOS (T) under contract to Department of the Environment of a two-dimensional
vertically integrated numerical model of current and sediment dynamics over the
Sizewell-Dunwich (S-D) Bank area of the southern North Sea. The model is now
almost at the stage where depth-averaged current velocities $\hat{U}$ can be accurately
predicted, given tidal elevation boundary conditions at the three open boundaries,
and the next step is to use these velocities to predict bed shear stresses τ_o
for insertion into sediment transport formulae. This informal report presents
the results of a two month study of the feasibility of making this step for the
general case of tidal flow over a sea bed with topography, with application to the
particular case of the S-D Bank.

The problem can be considered in two stages:

1. How accurately can a vertically integrated model predict bed shear stresses,
and would a three-dimensional model be appreciably more accurate.

2. Given accurate stresses, how successfully can they be used in sediment
transport formulae; and if the stresses are inaccurate what error in sediment
transport rates can be expected.

This investigation is chiefly concerned with the first of these questions. The
second is a topic which is of more general concern to the sedimentation side of
IOS (T) as a whole and will only be discussed briefly. The numerical model itself
might be used to explore some aspects of the second question.

I have tackled the first question from a number of standpoints:

(i)   survey of the relevant literature on analytical and numerical models.
(ii)   survey of the relevant literature on field observations
(iii) analysis of our own velocity profile measurements made in Lyme and Weymouth Bays
(iv)   analysis of Barbara Lees' velocity profile measurements made in the S-D Bank
area.

The area modelled is shown in Fig 1 where the coastline on the western boundary
has been artificially straightened for modelling purposes and the 8m depth contour
arbitrarily chosen to delimit the bank. Also shown are selected grid points of the
model, and the positions where velocity profile measurements have been made.
Typical values of the more important parameters together with their notation

are shown in Table 1. These values will be used throughout the report to assess
the magnitude of certain flow features when applied to the S-D Bank area.

Parameter	Symbol	Value	Comments
Length of bank	L	6 km	)
Width of bank	—	1 km	) At 8m contour
Water depth outside bank	h	10 m	)
Water depth over bank	—	5 m	
Tidal range	—	1.5 m	
Tidal frequency	σ	$1.40 \times 10^{-4} \text{rad.s}^{-1}$	
Coriolis parameter	f	$1.15 \times 10^{-4} \text{rad.s}^{-1}$	
Max depth averaged velocity	max $\hat{U}$	100 cm.s^{-1}	)
Max friction velocity	max U_x	5 cm.s^{-1}	)
Max bed shear stress	max τ_c	25 dynes.cm^{-2}	) From Marconi current
Drag coefficient	C_f	.0025	) meter data
Roughness length	z_0	.05 cm	)
Vertical eddy viscosity	K	$250 \text{ cm}^2\text{.s}^{-1}$	From Bowden et al (1959), Red Wharf Bay

Table 1: Typical values for the Sizewell-Dunwich Bank area

The full vertically integrated equations of motion are:

$$\underset{①}{\frac{\partial \hat{U}}{\partial t}} + \underset{②}{\hat{U}\frac{\partial \hat{U}}{\partial x}} + \underset{③}{\hat{V}\frac{\partial \hat{U}}{\partial y}} - \underset{④}{f\hat{V}} + \underset{⑤}{g\frac{\partial \zeta}{\partial x}} + \underset{⑥}{\frac{\tau_{cx}}{\rho h}} = 0 \qquad -1$$

$$\underset{⑦}{\frac{\partial \hat{V}}{\partial t}} + \underset{⑧}{\hat{U}\frac{\partial \hat{V}}{\partial x}} + \underset{⑨}{\hat{V}\frac{\partial \hat{V}}{\partial y}} + \underset{⑩}{f\hat{U}} + \underset{⑪}{g\frac{\partial \zeta}{\partial y}} + \underset{⑫}{\frac{\tau_{cy}}{\rho h}} = 0 \qquad -2$$

where $\hat{V}$ is the depth averaged velocity in the y direction, ζ the surface
elevation, g the acceleration due to gravity, ρ the water density, τ_c has been
resolved into τ_{cx} and τ_{cy}, and the remaining symbols are defined in Table 1.
The symbol $\hat{U}$ will be used to designate the weak east-west component of current
from the point of view of the model only; in the rest of the report the dominant
current will be designated $\hat{U}$. The advective terms $\hat{V}\partial\hat{V}/\partial y$ etc are a good
approximation to the integrals $\frac{1}{h}\int_{c}^{h} V\frac{\partial V}{\partial y} dz$ etc provided that the velocity
profile takes one of certain plausible forms. Horizontal diffusion of momentum
has been omitted from the equation for the present purposes, though for completeness
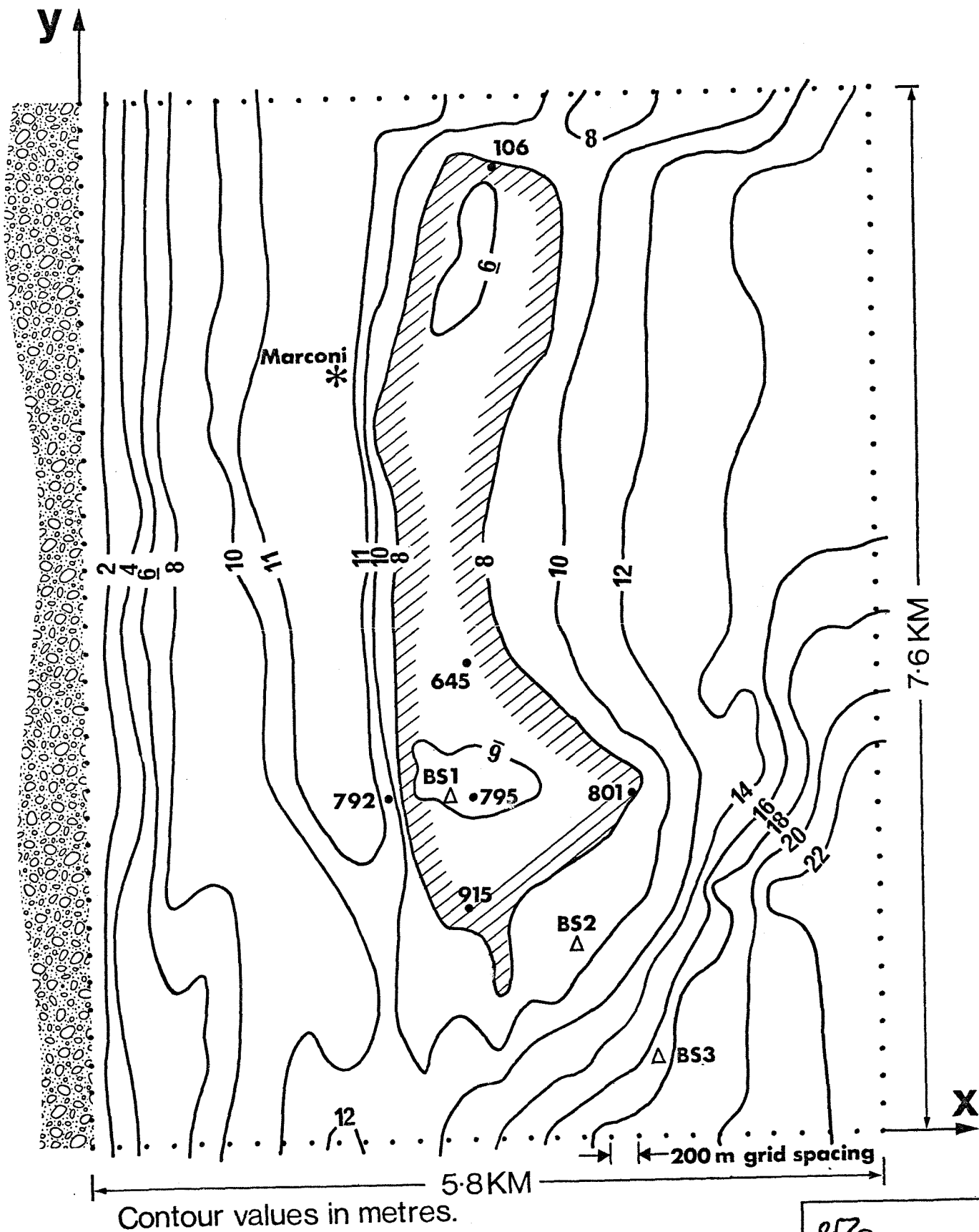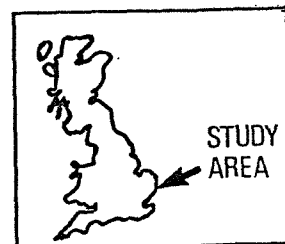this should also be estimated.

Fig. 1. Area covered by Sizewell-Dunwich Bank numerical
model, with coastline on west artificially
straightened. ● 106, selected gridpoints.
△ BS1, Braystoke current meter stations.
✳ Marconi current meter array position.

As a first step towards identifying the role of the various terms in the present context the model was made to produce time series of each of the terms throughout a tidal cycle at each of the selected representative gridpoints shown in Fig 1. The model was run with only the terms 1, 5, 6, 7, 11 and 12 included, as these were thought to be dominant, but the remaining terms were calculated from the values of $\hat{U}$ and $\hat{V}$ produced. $\mathcal{T}_{ox}$ and $\mathcal{T}_{oy}$ were calculated using a quadratic friction law as will be discussed later. Figs 2 - 7 * show that the y components on top of the bank (gridpoints 795 and 645) represent a balance principally between the friction and slope terms, with acceleration playing a secondary role and Coriolis being negligible. At the edges of the bank where the bed slopes steeply (gridpoints 106 and 792) the advective terms become important. Figs 8 - 13 * show that the modelled x components, the friction, slope and acceleration terms, are all small everywhere. The advective terms, particularly $\hat{V}\partial\hat{U}/\partial y$, are generally large, especially at the edges of the bank (gridpoints 792 and 801), and the Coriolis term is also important everywhere. The inclusion of the advective and Coriolis terms in the model will alter the balance of the terms, possibly in such a way as to alter their relative importance, but it is likely that the friction term will remain of primary importance so that its accurate modelling is important not just from the point of view of sediment transport but also for the prediction of $\hat{U}$ and $\hat{V}$. Various of the terms can be associated with the aspects of the relation between bed shear stress and depth averaged velocity which will be considered in the succeeding sections: the acceleration terms with the phase, the Coriolis terms with direction, and the advective terms with spatial development. As none of the terms is negligible, all the aspects need to be considered.

Bed shear stress is estimated by the S-D Bank numerical model, in common with the majority of vertically integrated models, using a quadratic friction law

* At end of report   3

$$\tau_o = \rho\, C_f\, \hat{U}\, |\hat{U}|$$

where the drag coefficient C_f is constant over the modelled area. Use

of this law assumes that the magnitude and direction of τ_c at a point in

space and at an instant in time is determined only by the magnitude and

direction of $\hat{U}$ at the same point and at the same instant. Question

1 above has been subdivided to investigate this into the questions

(i) Does τ_c exhibit any time lag or lead relative to $\hat{U}$

(ii) Is the direction of τ_c different to that of $\hat{U}$

(iii) Does topography introduce differences in the spatial
distributions of τ_c and $\hat{U}|\hat{U}|$

Questions (i) and (ii) are linked, as phase and direction are only

separable by making an artificial distinction, and some of the models

and observations described consider both. The distinction will generally

be classified by the context. The problem is fundamentally that of

the relationship between near-bottom currents and near-surface currents,

as U_* is closely related to the near-bottom currents, and $\hat{U}$ will be

dominated by the near-surface currents. In what follows the behaviour

of U_* will sometimes be approximated by that of the near-bottom currents,

and the behaviour of $\hat{U}$ by that of the geostrophic or free-stream velocity

U_∞ , the surface current U_S , or currents well away from the bed.

The quadratic friction law has been most extensively studied for the case

of steady flow over a flat boundary, so this will be summarised before

progressing to more complicated estimations. Steady turbulent flow over

a flat rough boundary produces a turbulent boundary layer which grows

downstream until it occupies the entire water depth. Near the boundary

the velocity profile has the familiar logarithmic form

$$U(z) = \frac{u_*}{k}\, \ln\left(\frac{z}{z_o}\right)$$

where $k \simeq 0.4$ is von Karman's constant and $\tau_o = \rho\, u_*^2$. Outside this the

velocity is greater than predicted by the log law, by an amount which for a smooth boundary is given by Coles' wake law (Monin and Yaglom, 1971). Assuming this to hold for a rough boundary gives

$$U(z) = \frac{u_*}{k} \ln\left(\frac{z}{z_0}\right) + \frac{u_*\Pi}{k}\left(1 - \cos\left(\frac{\pi z}{\delta}\right)\right) \quad for \quad z_0 \leq z \leq \delta \qquad -4$$

where δ is the boundary layer thickness, and Π a constant experimentally found to be 0.55 (Fig 14). Assuming fully developed flow (which it may not be), $\delta = h$, and using S-D Bank values indicates that the log profile alone is valid to better than 10% throughout the lowest 88% of the water depth. The lowest 15% of this contains a constant stress layer (Harvey and Vincent, 1977; Bradley, 1968). If the flow is very deep and time scales large, such as in the atmosphere or the deep ocean, the free stream flow is geostrophic, and the boundary layer no longer has to grow downstream but has a constant thickness $0.3\, u_*/f$. The velocity profile near the boundary follows the log law, whilst above this the velocity increases and veers to match the geostrophic flow at the top of the boundary layer, as described in Section 3. In the lowest portion of the log layer the shear stress is again roughly constant in both magnitude and direction throughout a layer of thickness $0.2\, u_*^2/U_\infty f$, where U_∞ is the geostrophic flow speed (Wimbush and Munk, 1970) Conditions in the S-D Bank, and over large areas of the continental shelf, lie between the extremes of the thin developing boundary layer and the full planetary boundary layer.

To help assess the important characteristics of the flow dynamics in the S-D Bank area a few scale lengths have been calculated (Table 2) using the numerical values given in Table 1.

Scale length. Thickness of:	Expression	Value for S-D Bank area	Comments
Viscous sub-layer	$12\,\nu/u_*$	.027 cm	for kinematic viscosity $\nu = \cdot 0114\ \mathrm{cm^2 s^{-1}}$
Constant stress layer	$0.15\,h$	1.5m	for 'developing' boundary layer
" " "	$0.2\,u_*^2/U_\infty f$	4.4m	for planetary boundary layer
logarithmic layer	–	7.7m	see text for expression
planetary boundary layer	$0.3\,U_*/f$	130m	see section 3
Ekman layer	$\pi\left(2K/f\right)^{1/2}$	66m	" " "
Stokes layer	$\pi\left(2K/\sigma\right)^{1/2}$	59m	see section 2

TABLE 2   Scale lengths for the Sizewell-Dunwich Bank area.

Sediment samples taken by Lees (1977) in the area reveal that over the bank the bed is composed of fine rippled sand which probably has a ripple height of somewhere between 1cm and 3cm.   This is large compared with the viscous sublayer thickness so that the flow will be hydrodynamically rough for most of the tidal cycle.   To the west of the bank the bed has a veneer of fine sand of diameter about 180 μm which is probably not rippled so that here the flow regime will be transitional.   To the east there is gravel of maximum length 8cm where the flow will again by hydrodynamically rough.

The water depth is small, but not negligible, in comparison with the thicknesses of the planetary boundary layer, Ekman layer and Stokes layer, so that direction and phase differences between τ_c and $\hat{U}$ are likely to be correspondingly small but not negligible.

PHASE DIFFERENCE BETWEEN τ_c AND $\hat{U}$

The use of a quadratic friction law relies on an assumption that u_* is in phase with $\hat{U}$ throughout the tidal cycle, but it is easily seen that this need not be so.   The equation of motion for the U component of velocity for a sea uniform in the horizontal directions over a flat horizontal bed
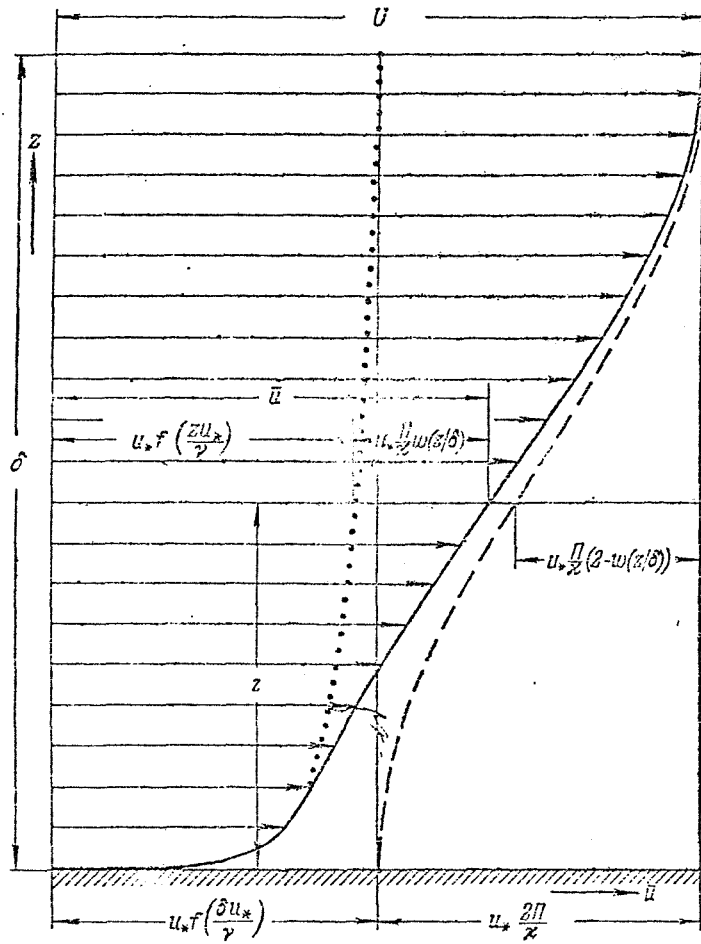
6

Fig 14. Schematic representation of the velocity profile satisfying Coles' wake law (from Monin and Yaglom, 1971)

omitting Coriolis terms reduces to

$$\frac{\partial U(z)}{\partial t} = -g\frac{\partial \zeta}{\partial x} + \frac{1}{\rho}\frac{\partial \tau}{\partial z} \qquad\qquad - 5$$

where ζ is the surface elevation and τ the shear stress. At a height $z = s$ well away from the bed we will assume that the effect of friction can be neglected, so that

$$\frac{\partial U(s)}{\partial t} = -g\frac{\partial \zeta}{\partial x} \qquad\qquad - 6$$

If the friction term at a height $z=b$ near to the bed is linearised and assumed to be proportional to and in phase with the near-bed velocity, then

$$\frac{1}{\rho}\frac{\partial \tau}{\partial z}\Big|_{z=b} = -A(b)\,U(b) \qquad\qquad - 7$$

where A is a dimensional positive function of z , so that

$$\frac{\partial U(b)}{\partial t} = \frac{\partial U(s)}{\partial t} - A(b)\,U(b) \qquad\qquad - 8$$

Inserting a sinusoidal tidal time dependence $U(s) = U_{so}\cos\sigma t$ and $U(b) = U_{bo}\cos(\sigma t + \varepsilon)$ and re-arranging shows that $U(b)$ leads $U(s)$ by a phase $\varepsilon = \arctan\left(A(b)/\sigma\right)$ which is ~~passib~~ positive as A is positive. τ_o is in phase with $U(b)$, and $\hat{U}$ is approximately in phase with $U(s)$ for typical velocity profiles, so τ_o must lead $\hat{U}$.

In cases where the terms omitted from the equation of motion above are retained, or where the friction term is nonlinear, it is not always possible to define a phase difference, as τ_o is no longer sinusoidal. In what follows, the term 'phase' is sometimes used in connection with these cases and should be understood to mean the phase of the dominant harmonic of τ_o , or for a quadratic friction law, of U_{*} .

The theoretical treatment of the problem can be developed by expressing the friction term in eq. 5 using an eddy viscosity approach. In the

simplest cast Lamb (1975) assumes that the eddy viscosity K is constant throughout the water depth h and also constant in time. This is a particular case of the Stokes shear wave problem, and for our present purposes the solution for U can be integrated from $z=0$ to $z=h$ to give

$$\hat{U} = \int_0^h U \, dz$$
$$= R_1 \exp(i\hat{\phi_1}) \qquad\qquad - 9$$

where $R_1 = \dfrac{P_0}{\sigma} \left[\{ b(\cosh b + \cos b) - (\sinh b - \sin b) \}^2 + \{ \sinh b - \sin b \}^2 \right]^{1/2} \Big/ b(\cosh b + \cos b)$

and $\quad b = \left(\dfrac{2\sigma h^2}{K} \right)^{1/2}$

Taking the derivative of the solution for U with respect to z evaluated at the bed

$$\tau_0 = K \frac{\partial u}{\partial z} \Big|_{z=0}$$
$$= R_2 \exp(i\hat{\phi_2}) \qquad\qquad - 10$$

where $\quad R_2 = P_0 \left(\dfrac{\sigma}{K} \right)^{1/2} \left(\sinh^2 b + \sin^2 b \right)^{1/2} \Big/ (\cosh b + \cos b)$

and $\quad \hat{\phi_2} = \sigma t - \dfrac{\pi}{4} + \arctan(\sin b / \sinh b)$

Thus τ_0 leads $\hat{U}$ by a phase angle $\varepsilon = \hat{\phi_2} - \hat{\phi_1}$. The functional dependence of ε on b is shown in Fig 15. In the limit as $h \to 0$ the shear stress is in phase with the depth-averaged velocity. As the water depth increases the shear stress exhibits a phase lead over the depth-averaged velocity, tending towards a lead of 45° as $h \to \infty$.

For the case of infinitely deep water a suitable scale height z_{st} is given by the height at which the fractional departure from the free stream flow is $e^{-\pi}$,

$$z_{st} = \pi \left(\dfrac{2K}{\sigma} \right)^{1/2} \qquad\qquad - 11$$

The value of b using S-D Bank values is 1.06, which from Fig 15 corresponds
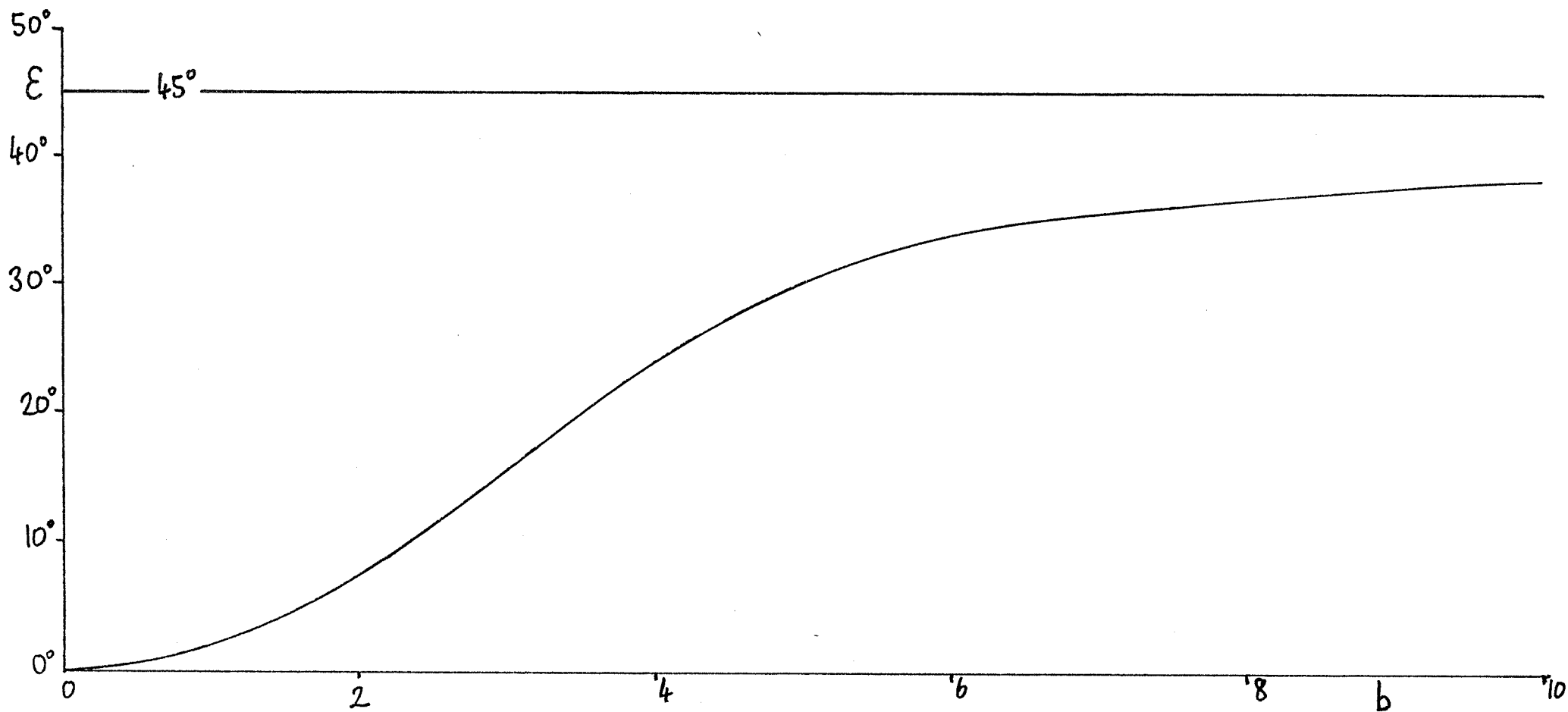
Fig 15. Phase ε by which τ_o leads $\hat{U}$ for the Stokes shear wave as a function of $b = (2h^2\sigma/\nu)^{1/2}$.

Also angle by which τ_o is anticlockwise of $\hat{U}$ for the Ekman spiral as a function of $b_{EK} = (2h^2 f/\nu)^{1/2}$.

to τ_c leading $\hat{U}$ by 1.9° (1° is about 2 mins for the semidiurnal period).

A more realistic form for the eddy viscosity is used by Smith (1977a) who takes K to increase linearly with distance from the bed but still to be independent of time. The boundary conditions used are those corresponding to an infinitely deep sea. Inserting S-D Bank values into his solution indicates that τ_c leads $\hat{U}_{\infty} \simeq \hat{U}$ by 8°, but it is likely that if more suitable boundary conditions corresponding to a shallow sea were used in the solution this value would be much reduced. Bowden et al (1959) include a Coriolis term in a two layer model in which K is taken as constant in the upper layer which occupies the top 90% or so of the flow depth, and the lower friction layer is used solely to provide a boundary condition at the interface between the layers. Numerical values corresponding to Red Wharf Bay are used which are very comparable to those for the S-D Bank area, and his results show that τ_c (taken as equal to the stress at the interface) leads $\hat{U}$ by 1.6°.

A considerable body of work on the numerical solution of shear wave problems has been produced by Johns, both as applied to shallow-water surface waves (1975, 1977) and to tidal flow in estuaries (1969, 1970, 1976). Throughout the work the friction term is treated using a mixing length approach, with the mixing length being a specified function of height above the bed, whose form is chosen to suit the particular problem. The effect of introducing a phase difference between τ_c and $\hat{U}$ is discussed by Johns (1969), but none of the consequences (such as energy dissipation) discussed lead to a prediction of whether the phase should be positive or negative. A prediction that τ_c leads $\hat{U}$ can be inferred from velocity profiles presented by Johns (1976), although neither τ_c nor $\hat{U}$ is actually plotted in this paper. The time-dependence of τ_c throughout a wave-cycle is given specifically by Johns (1977),

in which the turbulent kinetic energy equation is introduced into the system

of equations governing the boundary layer dynamics beneath waves so as to

allow transfer and dissipation of turbulence energy.   Fig 16 reproduces

this, and it is seen that the time variation of $\widetilde{\tau_c}$ is not simple, nor

is it approximated well by a quadratic friction law.   However, it is not

clear how this should be interpreted for the present case of tidal flow

in water of limited depth.

An attractive treatment is given by Vager and Kagan (1969) who include

Coriolis terms in the equations of motion and effect closure at the level

of the turbulent energy equation without assuming an artificial functional

dependence for mixing length.   Unfortunately the results of the model are

presented for only one particular case, and this with a minimum of discussion.

For a maximum surface velocity of 100 cm s^{-1}, comparable with the S-D Bank,

this case would correspond to a water depth of 70m, which is much deeper

than the S-D Bank$_\Lambda$. It can be roughly estimated from their diagrams that for

this case $\widetilde{\tau_c}$ leads $\overrightarrow{U}$ by approximately 20°.

A very similar approach is used by Weatherly (1975) to model the Florida

Current.   The results are discussed in more detail than those of Vager and

Kagan (1969), but are not directly comparable to the S-D Bank case, as

(i) the Florida Current has a residual flow equal in magnitude to the

tidal component, so that the current speed drops to zero but does not

reverse, (ii) the dominant tidal component is diurnal, (iii) the depth is

sufficiently great (800m) that a full planetary boundary layer can develop,

(iv)the flow was stratified, (v) the model was not run for sufficiently

long to allow all transients to disappear.   A plot of U_x against time is

given, and this has been rearranged to give the plot of U_x against the

free stream velocity, U_∞, shown in Fig 17.   It can be seen that U_x leads

U_∞ by an amount which can be roughly estimated from the original data

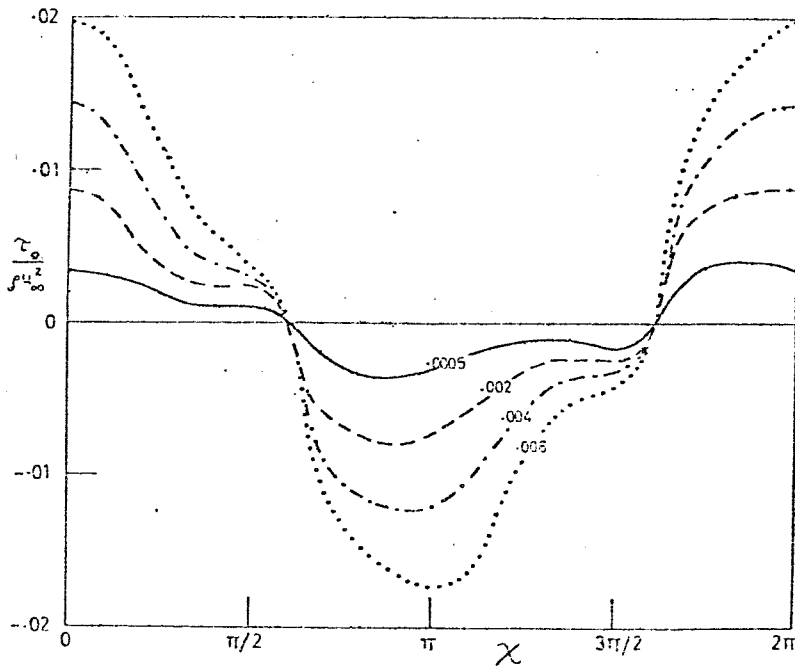as about 26°.   The variation throughout a tidal cycle of the ratio

Fig 16. The variation of τ_o through one cycle of a wave of period $6\cdot28$s in water of depth 1m for different values of non-dimensional roughness length (from Johns 1977).
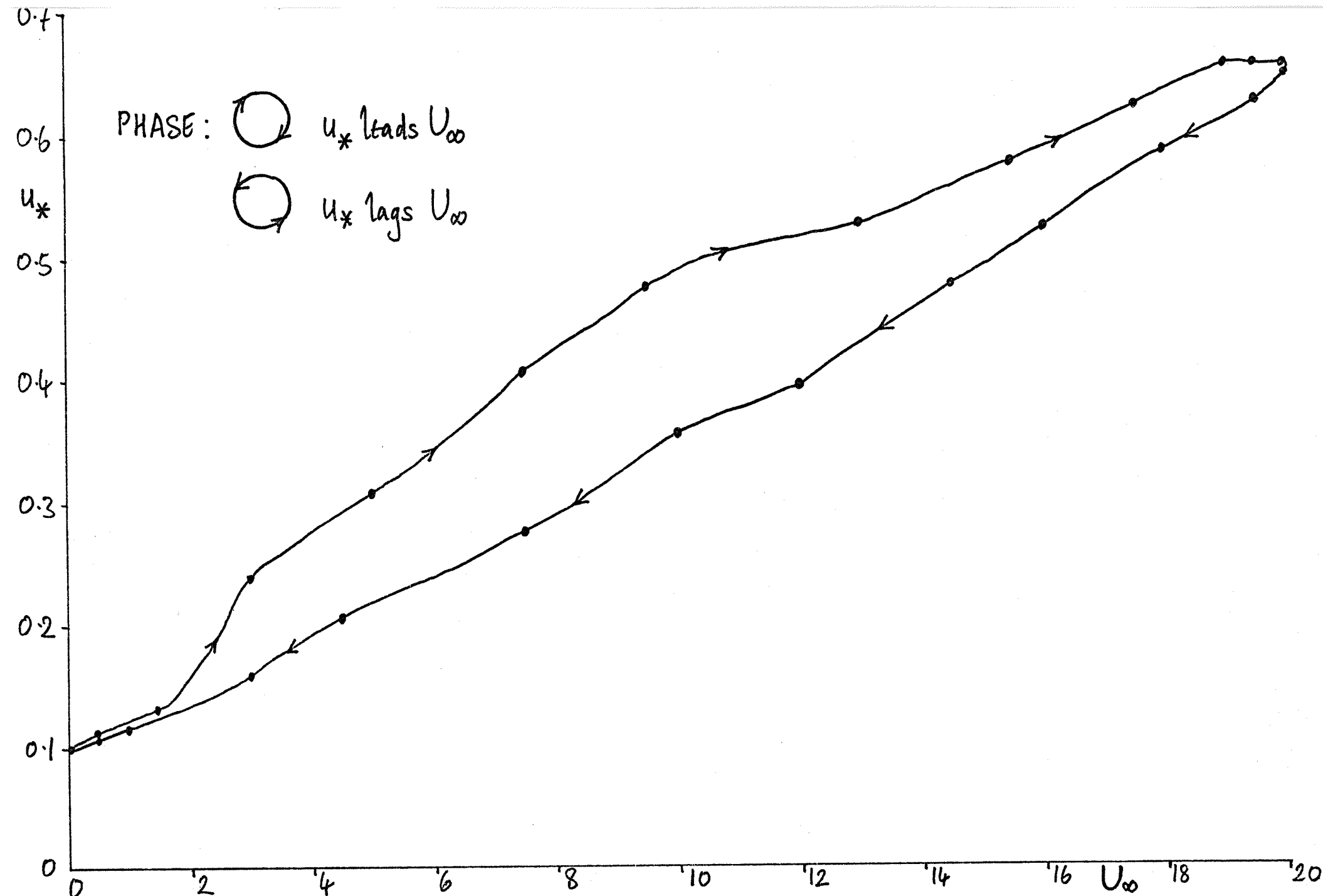
Fig 17. Dependence of u_* on U_∞ as predicted by Weatherly's (1975) model of the Florida Current. Dots indicate hourly values.

$u_*/U_\infty \equiv (C_f)^{1/2}$ is shown in Fig 18. It is clear that near the start and end of the cycle, U_∞ decreases faster than u_* so that $(C_f)^{1/2}$ takes large values. It is of particular interest to note that the thickness of the boundary layer as determined by the model is very different in both amplitude and phase to that predicted for a quasi-stationary situation.

Turning now from models of tidal flow to field observations we find that the velocity profiles of Bowden et al (1959) indicate qualitatively that the near-bed velocity leads the velocity higher up in the flow. Wei sberg and Sturges (1976) analysed current measurements made in a partially mixed estuary (Narra gansett Bay) in 12.8m of water, and found that velocities at 5.6m above the bed led those at 10.7m above the bed by about $9^o - 13^o$. They found good agreement with a simple Stokes shear wave model, though the eddy viscosity they used was only $8cm^2s^{-1}$ which seems rather low, and it is perhaps more likely that density stratification might account for some of the observed lead. Harvey and Vincent (1977) found that their measurements in the southern North Sea in 35m of water were consistent with the near-bed currents leading those well above the bed, but did not indicate by how much. Measurements made by Pingree and Griffiths (1974) on the edge of the continental shelf SW of Lands End in 188m of water indicated a 13° phase lead of the currents at 3.5m above the bed relative to those 98m above the bed for the semi diurnal tidal component. This lead was mainly attributed to the thermocline descending semidiurnally below 98m, though it seems plausible that the inertia-friction effects discussed in this section xxxkx would also contribute.

There are also a number of investigators who have found that the near bottom currents lag behind those nearer the surface. Channon and Hamilton (1971) analysed measurements made at a number of sites in the western English Channel and the Bristol Channel in water depths ranging from 14m to 104m with maximum tidal current speeds ranging from about $2cm \ s^{-1}$ to 97 cm s^{-1},

and concluded that there was an appreciable phase lag of bottom current fluctuations that behind those occurring nearer the surface. Gordon (1975) measured the Reynolds stress and mean velocity 2.25m above the bed in the Choptank estuary in 8m of water with maximum tidal currents of 70 cm s^{-1}, and presented evidence that the stress lagged the mean velocity by a phase which can be estimated from his diagrams as 29°. He attributed this to an increase in the turbulent burst rate during periods of adverse pressure gradient such as occur in decelerating tidal flow, though there is possibly some confusion here between the effects of pressure gradients and those of spatial accelerations. Indirect evidence is provided by the sediment concentration measurements of Thorn (1975) at various heights in the Thames estuary where the water depth was 19m and maximum tidal velocities were about 110 cm s^{-1}, who found that the sediment concentration lagged behind the mean current velocity. This was attributed to the finite time taken for sediment to diffuse upwards and to settle out, though a lag in the shear stress relative to the mean velocity could be a contributory factor. This is discussed further by Davies (1977).

Our own measurements made over a flat uniformly rough bottom in Weymouth Bay, where the water depth was 28m and tidal currents reached 75 cm s^{-1} have been examined in terms of the phase problem. U_{*} was estimated from near-bed velocity profiles averaged over successive 12 min periods, and $\hat{U}$ is approximated by U_{S-5}, the velocity 5m below the water surface, which was read every 30 mins. U_{*} is plotted against U_{S-5} in Fig 19, and clearly shows that U_{*} leads U_{S-5} by a phase which can be roughly estimated as 10°.

Finally we consider current measurements made in the S-D Bank area at a site shown in Fig 1, where the water is 12.2m deep and the maximum tidal current is about 90 cm s^{-1}. Measurements were obtained from Marconi current meters mounted 1.2m, 3.2m, 4.2m and 6.2m above the bed over a period covering almost
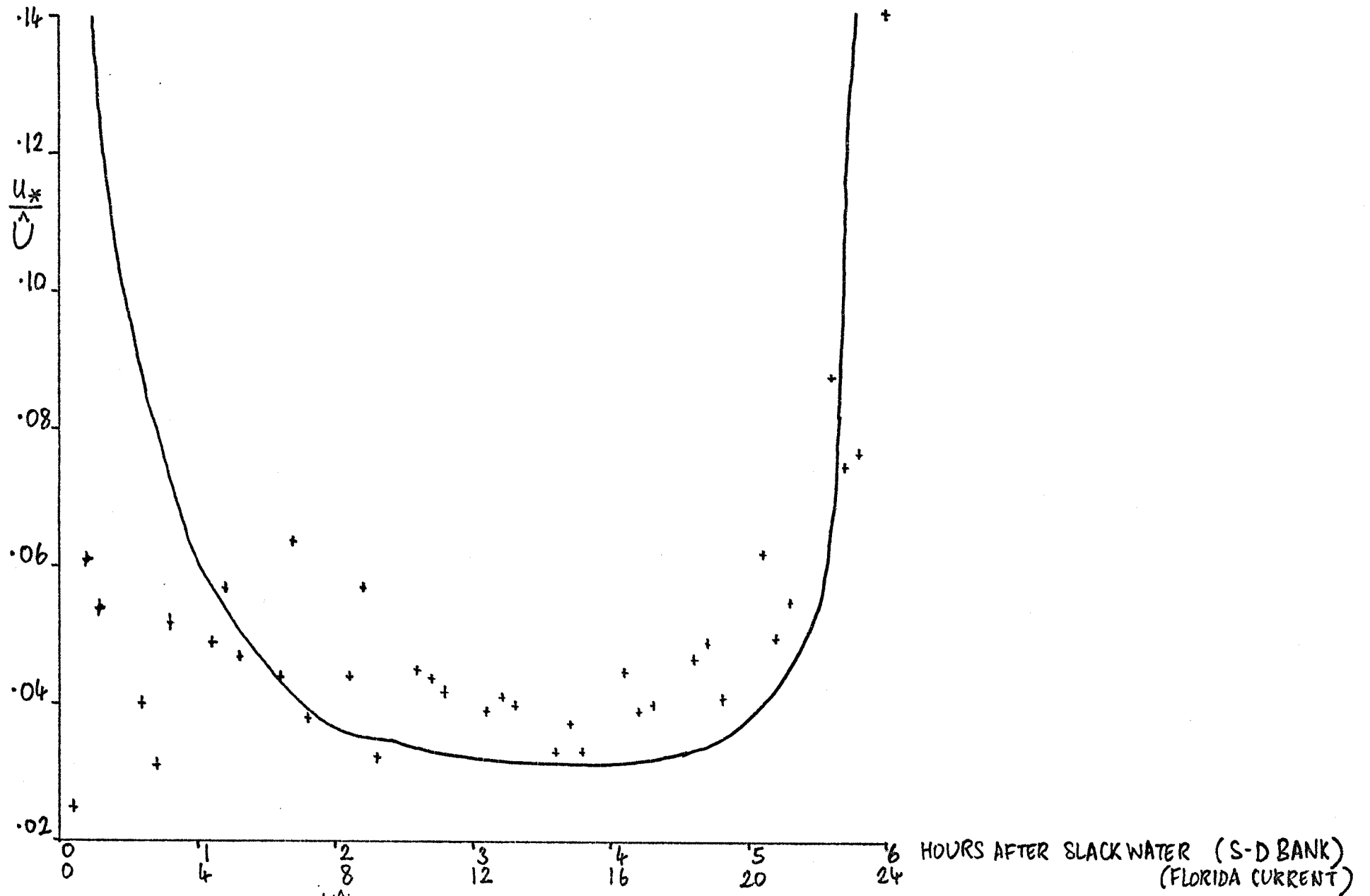
Fig 18. Variation of $u_*/\hat{U}$ through tidal cycle . Crosses, S-D Bank data; line, Florida Current as predicted by Weatherly's (1975) model.

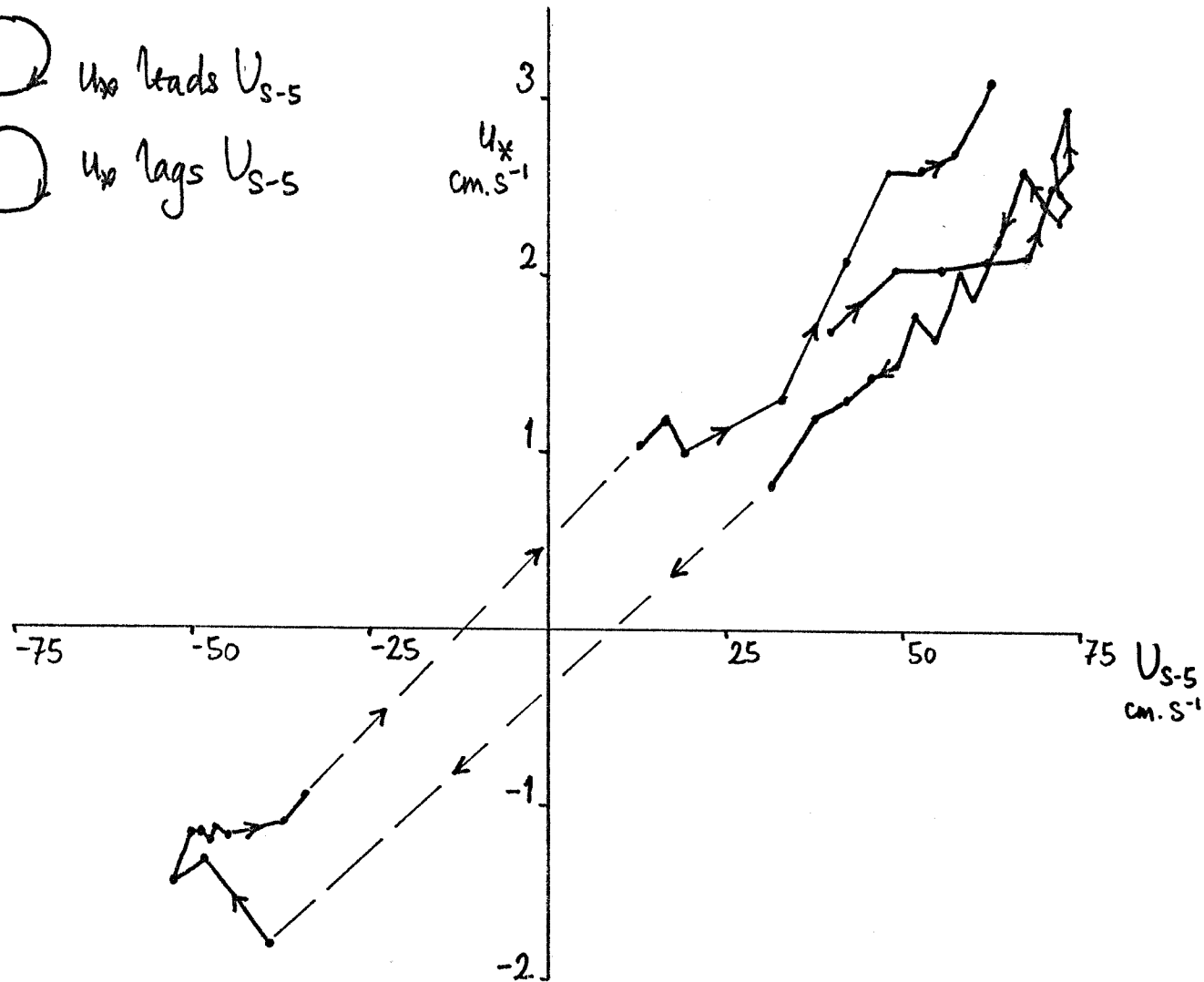PHASE: u_{*} leads U_{s-5}

u_{*} lags U_{s-5}

Fig 19. Dependence of u_{*} on the mean velocity 5m below surface, U_{s-5}, for Weymouth Bay. Dots indicate half-hourly values.

four tidal cycles. To examine the data for phase differences the measurements were averaged over successive 30min periods, U_{x} estimated from the measurements at 1.2m and 3.2m by assuming that the velocity profile is logarithmic up to 3.2m, and $\hat{U}$ estimated by assuming a logarithmic velocity profile up to 3.2m, a parallelogram rule up to 6.2m, and constant velocity above that. The assumption of a logarithmic profile up to 3.2m was shown to be satisfactory by comparing the U_{x} values with those obtained from measurements at 1.2m and 2.2m over a period of 1 hr when a meter at 2.2m was working. Values of $\hat{U}$, U_{x} and $C_f = \left(U_{x}/\hat{U}\right)^{2}$ are plotted for the four tidal cycles in Fig 20. U_{x} is seen to exhibit a 'dwell' after the maximum, which is similar in form to that found by Johns (1977) and shown here as Fig 16. The drag coefficient C_f is reasonably steady around a value of about 2×10^{-3} over most of each half cycle, but increases rapidly as slack water is approached. The ratio $U_{x}/\hat{U}$ is plotted against phase of the tide in Fig 18 for the first three half cycles, and is found to agree quite well with the curve predicted by Weatherley's (1975) model, apart from the time just after slack water.

U_{x} is plotted against $\hat{U}$ in Figs 21$_{x}$-24, from which it can be seen that U_{x} is not related to $\hat{U}$ in a simple way. Considering a clockwise progression on Fig 21 to indicate U_{x} leading $\hat{U}$ and vice versa, there is a consistent pattern throughout the four tidal cycles of U_{x} leading $\hat{U}$ at times of maximum flow, but U_{x} lagging $\hat{U}$ when velocities are smaller. The reason for this may be associated with the Johns-like behaviour referred to above, or may be connected with the presence of the sand bank. It is not appropriate to estimate a value for the phase difference under the circumstances. The average value of C_f over the first tidal cycle was found to be .0022 from a linear regression of ~~xxxxx~~ ~~thexfirstxtidalxcyclexwa~~ $U_{x}|U_{x}|$ on $\hat{U}|\hat{U}|$, and the average value of $\ln\left(z_0/1cm.\right)$ taken over the same period but excluding a few rogue values was found to be -2.973, yielding an average value of z_0 = .051 cm.

The presence of ripples on the bed is the cause of a similar but distinct problem. In areas of mobile sand the bed is likely to be rippled which will increase the total bed shear stress, but the ripple pattern, and hence the drag coefficient, will change throughout the tidal cycle. Recent work by Keith Dyer suggests that this may occur in Start Bay. It is possible that this could be responsible for the complicated behaviour of u_x at the S-D site discussed above, though it is not known whether the bed at this site is rippled. The low value of z_0 suggests it is not. However, on the bank itself, it is expected that the bed is rippled.

DIFFERENCE IN DIRECTION BETWEEN τ_0 AND $\hat{U}$

Some of the models and observations considered in the last section take account of the effects of the earth's rotation, one consequence of which is that τ_0 and $\hat{U}$ need not be in the same direction. The subject has been considered in some detail since the classical work of Ekman (1905) although more attention has been devoted to the case of a wind-induced surface current than to the bottom boundary layer, and to the steady rather than to the time-dependent case. In the time-dependent case the veering will, in general, also be time-dependent.

It is useful to recognise an analogy between the problem of the steady bottom boundary layer with Ekman veering, and the oscillatory boundary layer discussed in the previous section. In both cases a horizontally homogeneous ocean of infinite extent but finite depth h is assumed. For the case of the oscillatory boundary layer with a periodic forcing function X_{st} (Stokes case) the equation of motion neglecting the Coriolis term is

$$\frac{\partial U_{st}}{\partial t} = \frac{\partial}{\partial z}\left(K(z,t)\frac{\partial U_{st}}{\partial z}\right) + X_{st}$$

- 12

If X_{st} and U_{st} both have an $\epsilon \circ (i\sigma t)$ time dependence, then

14
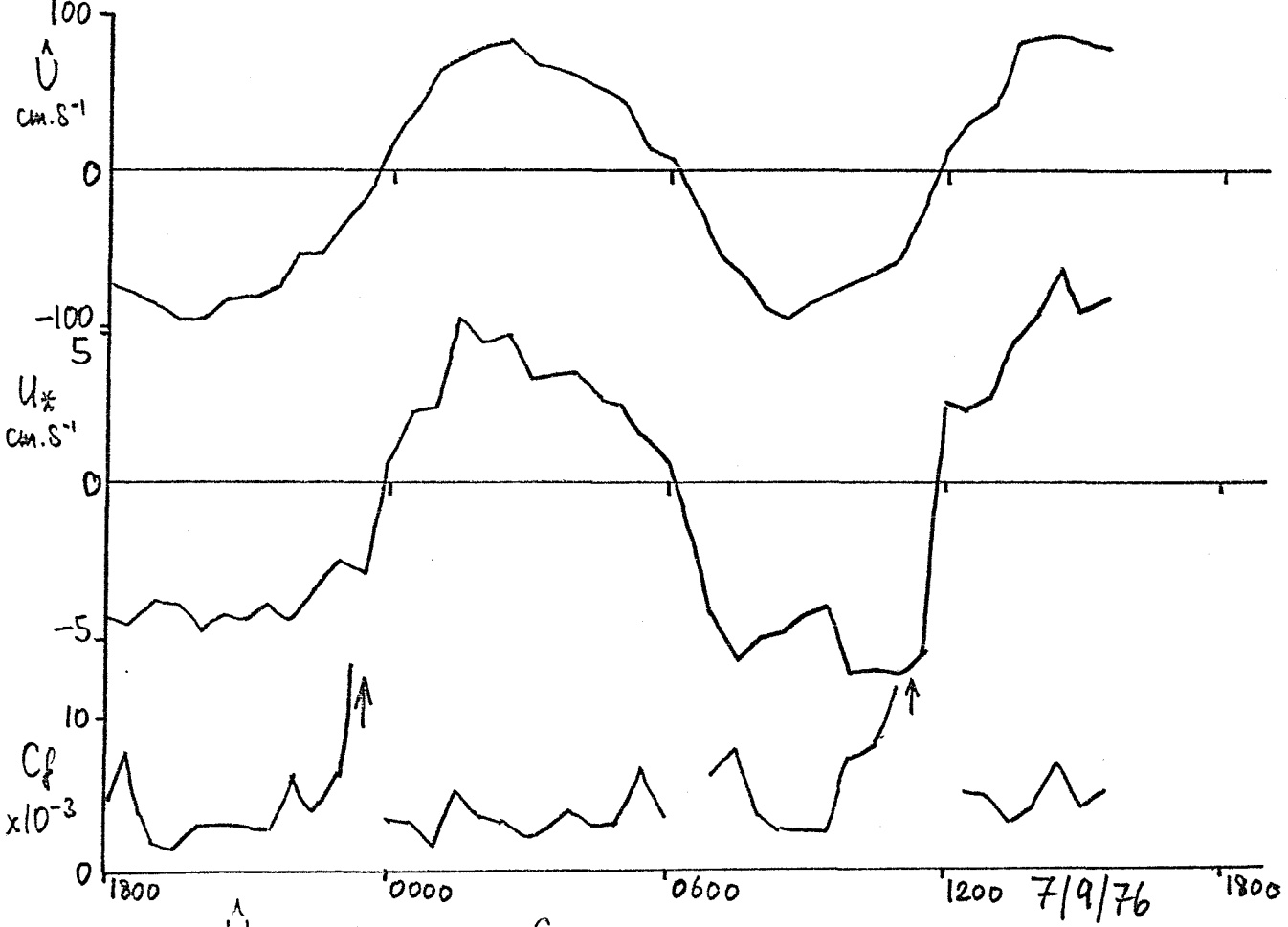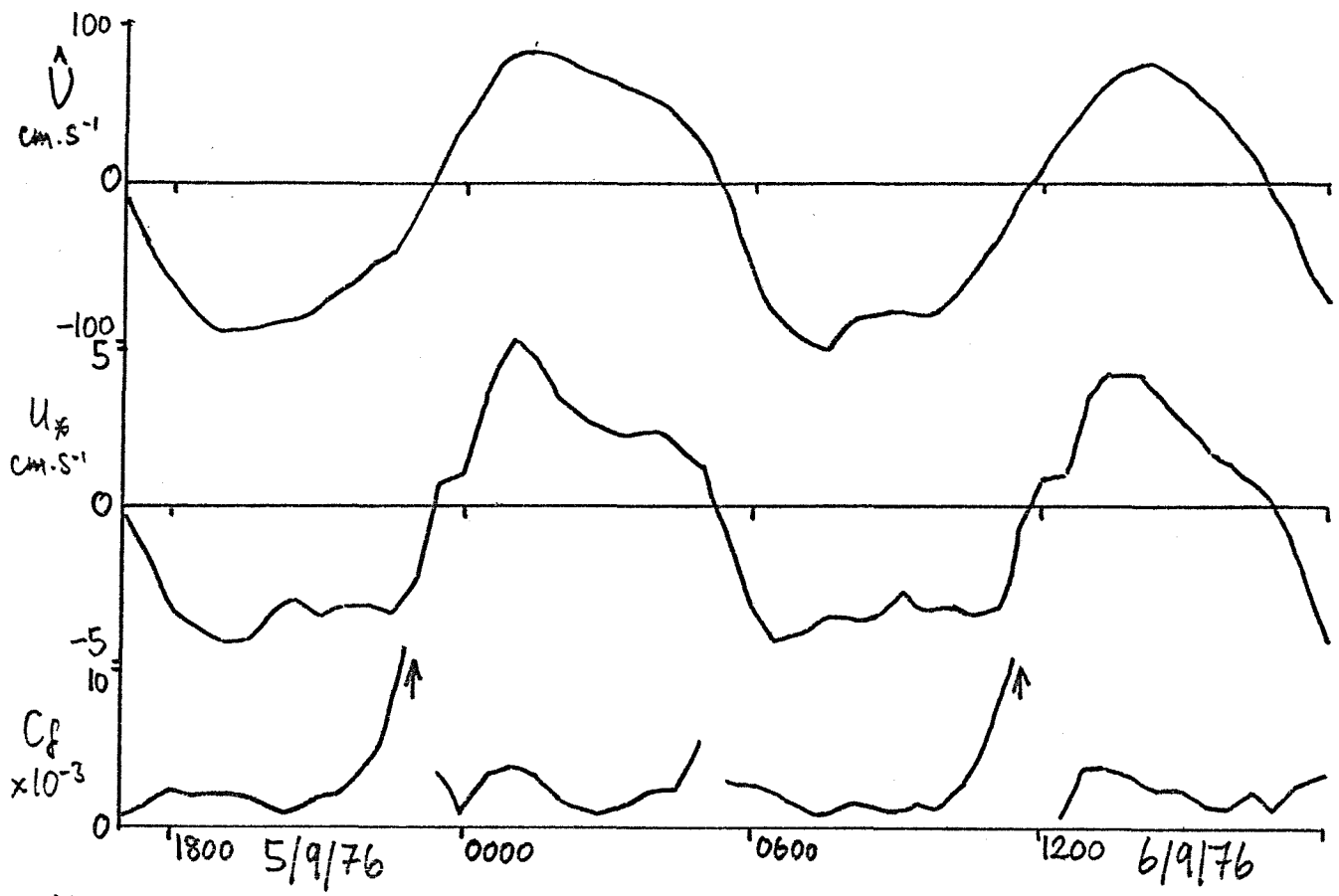
Fig 20. $\hat{U}$, u_* and C_f for the S-D Bank Marconi current meter data.

Phase:

u_* leads $\hat{U}$

u_* lags $\hat{U}$

Fig 21. Dependence of u_* on $\hat{U}$ for the S-D Bank Marconi current meter data. Dots indicate half-hourly values over period 1700 BST on 5 September 1976 to 0530 on 6 September 1976.

Fig 22. Dependence of u_* on $\hat{U}$ for the S-D Bank Marconi current meter data. Dots indicate half-hourly values over period 0530 to 1700 BST on 6 September 1976.
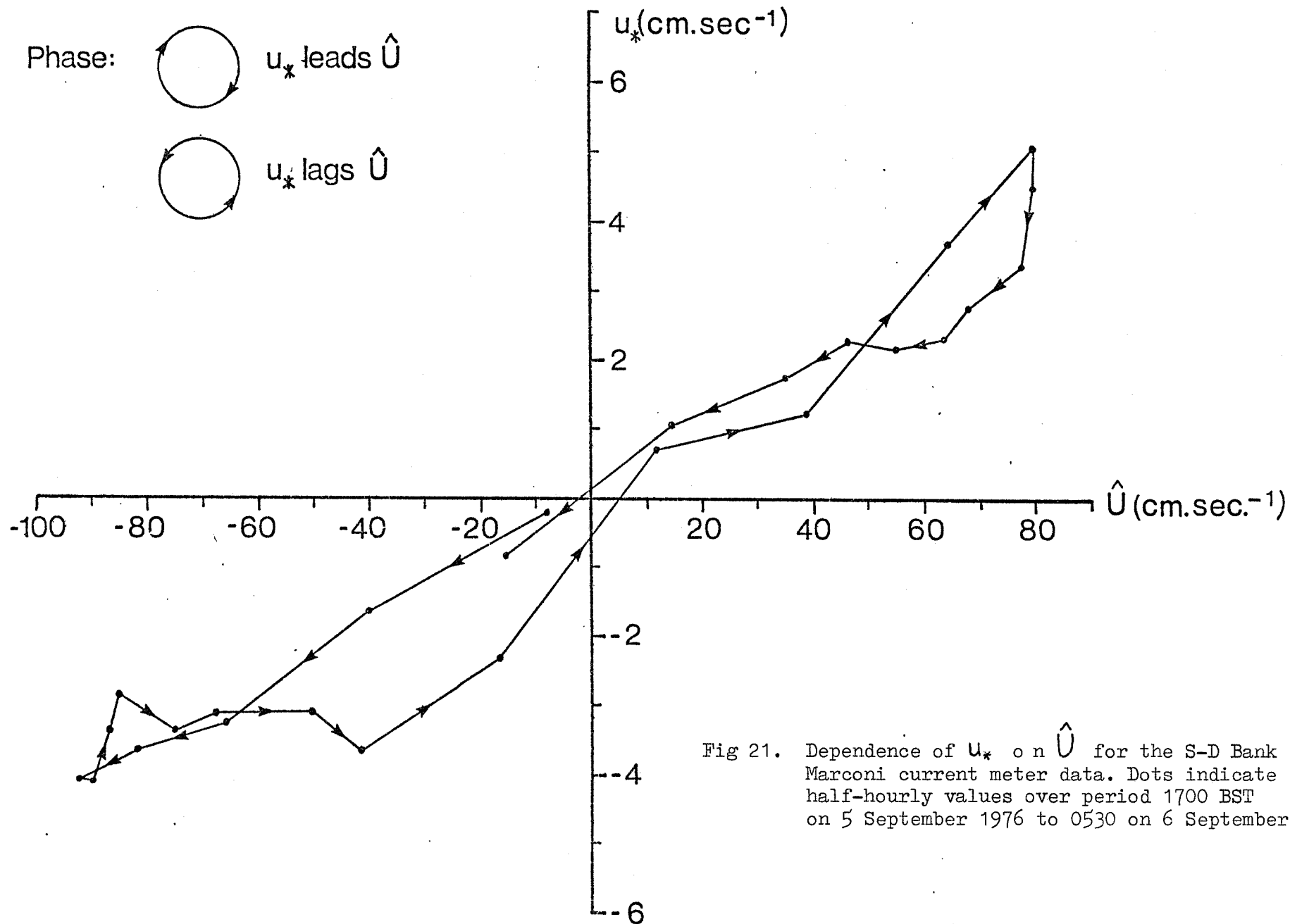
Fig 23. Dependence of u_* on $\hat{U}$ for the S-D Bank
Marconi current meter data. Dots indicate
half-hourly values over period 1700 BST
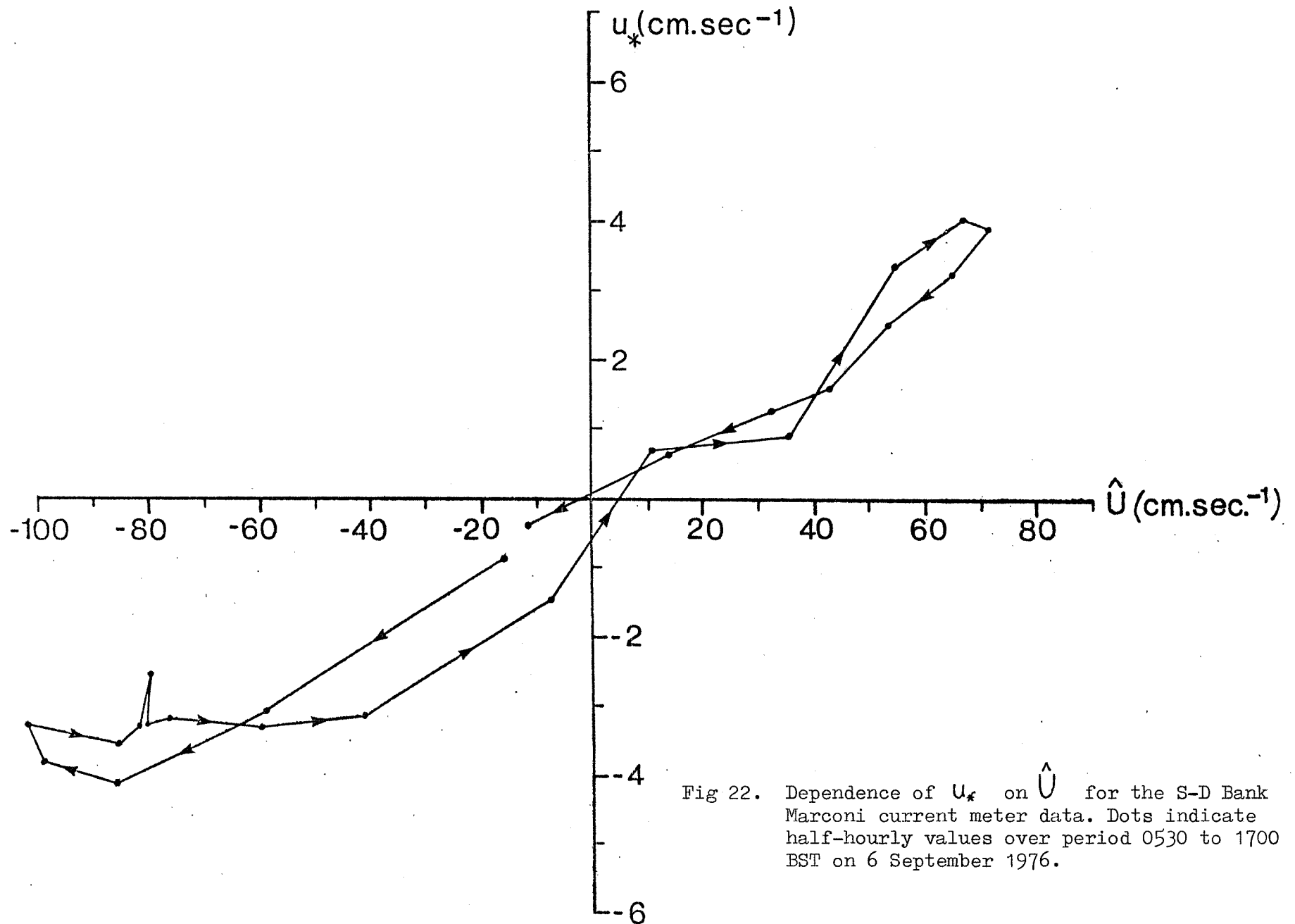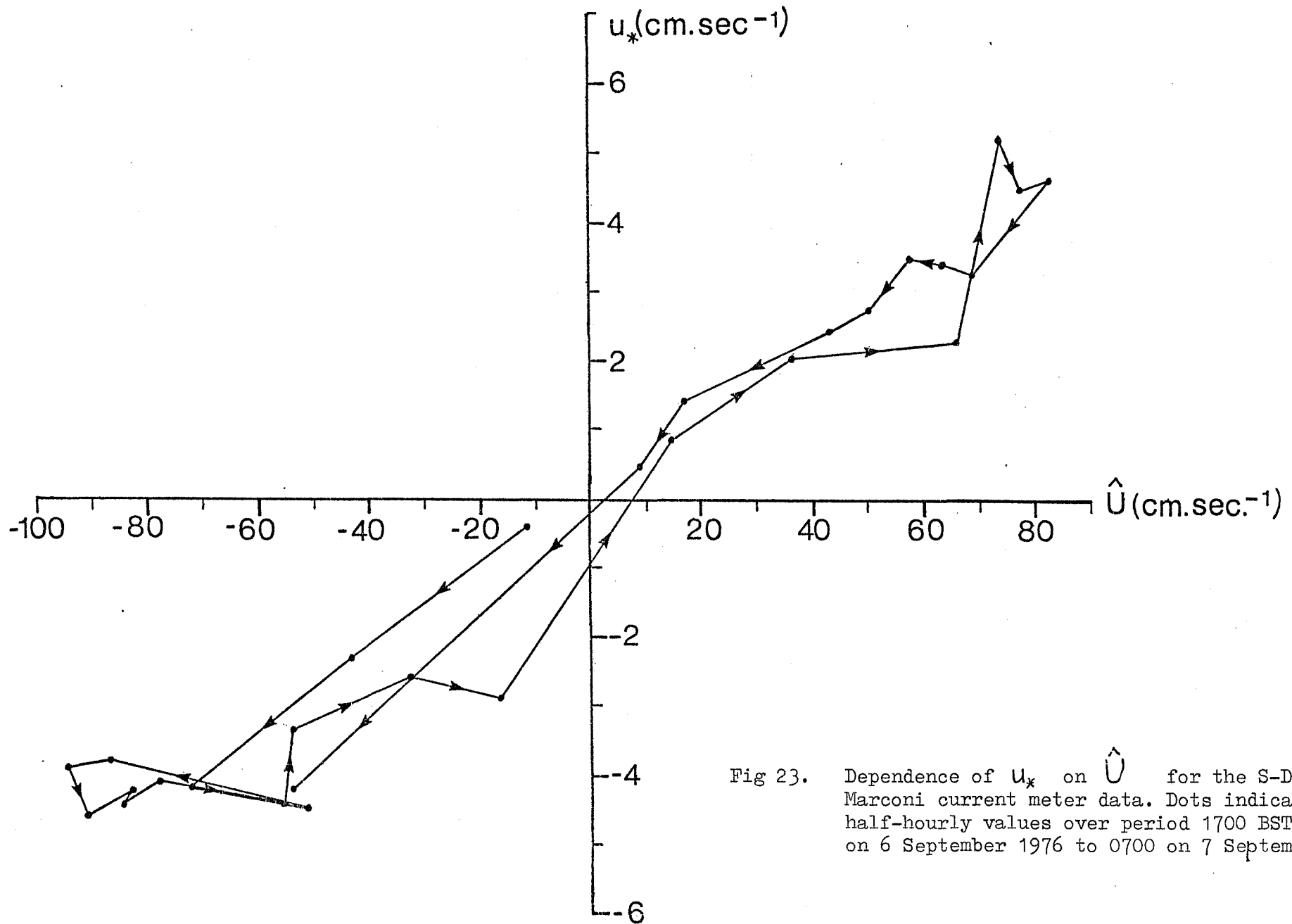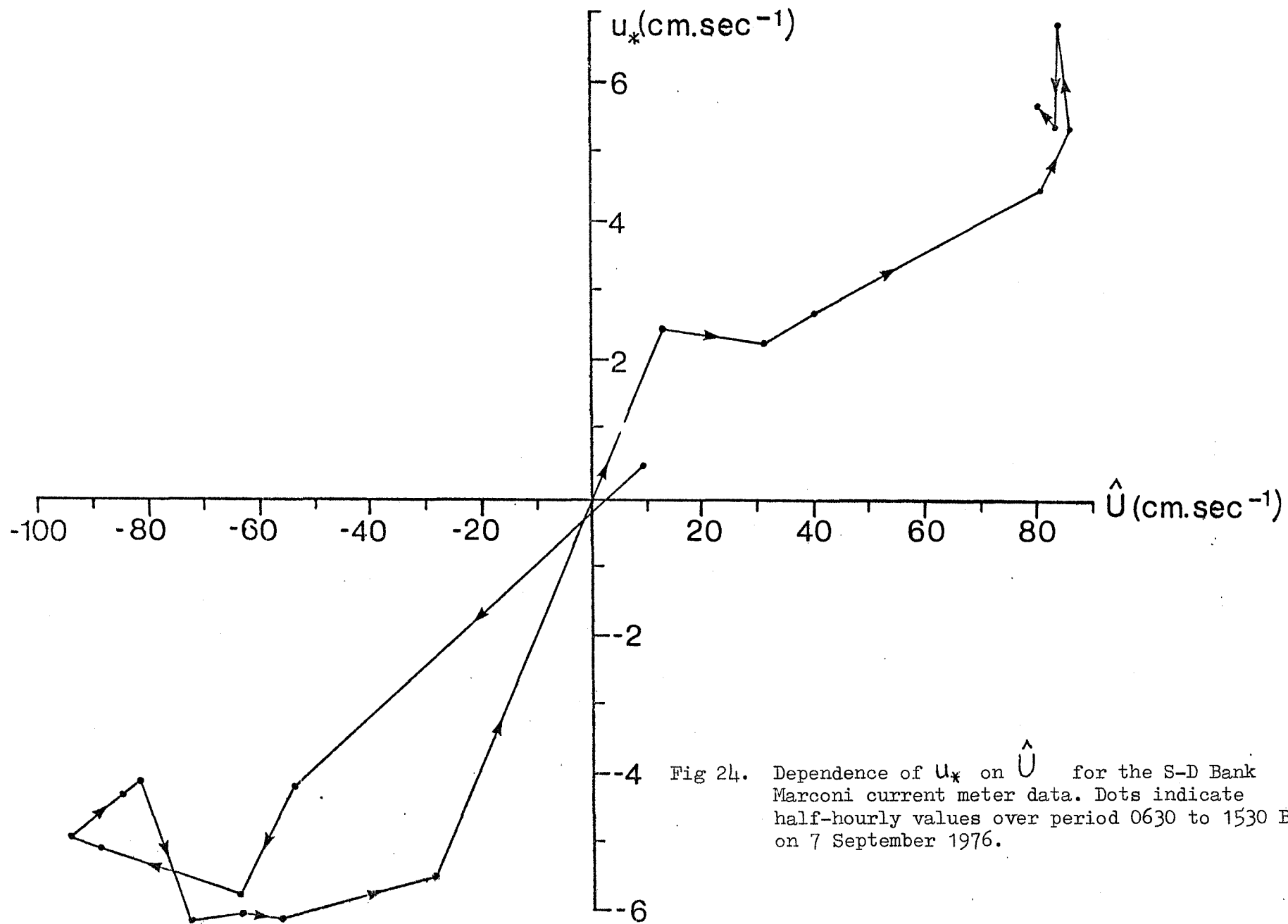on 6 September 1976 to 0700 on 7 September 1976.

Fig 24. Dependence of u_* on $\hat{U}$ for the S-D Bank Marconi current meter data. Dots indicate half-hourly values over period 0630 to 1530 BST on 7 September 1976.

$$i\sigma U_{st} = \frac{\partial}{\partial z}\left(K \frac{\partial U_{st}}{\partial z}\right) + X_{st} \qquad \text{- 13}$$

with boundary conditions $U_{st} = 0$ at $z = 0$ and $\frac{\partial U_{st}}{\partial z} = 0$ at the water surface $z = h$. The phase of U_{st} is given by $\tan^{-1}\left(Im(U_{st})/Re(U_{st})\right)$.

The equations of motion of a bottom boundary layer driven by a steady force X_E including Coriolis terms (Ekman case) are

$$-f V_E = \frac{\partial}{\partial z}\left(K(z,t) \frac{\partial U_E}{\partial z}\right) + X_E \qquad \text{- 14}$$

$$f U_E = \frac{\partial}{\partial z}\left(K(z,t) \frac{\partial V_E}{\partial z}\right) \qquad \text{- 15}$$

where $f = 2\Omega \sin\phi$ is the Coriolis parameter, Ω the earth's angular frequency and ϕ the latitude. Writing $\xi_E = U_E + i V_E$, multiplying the second equation by i and adding it to the first equation gives

$$i f \xi_E = \frac{\partial}{\partial z}\left(K \frac{\partial \xi_E}{\partial z}\right) + X_E \qquad \text{- 16}$$

Here the boundary conditions are $\xi_E = 0$ at $z = 0$ and $\frac{\partial \xi_E}{\partial z} = 0$ at $z = h$. In the Ekman case the azimuth of ξ_E is given by $-\tan^{-1}\left(Im(\xi_E)/Re(\xi_E)\right) \equiv -\tan^{-1}\left(\frac{V_E}{U_E}\right)$ Equations 13 and 16 are identical in form, and moreover the values of σ and f are fairly similar for a semidiurnal tide in temperate northern latitudes, so that the phase difference between τ_0 and $\hat{U}$ will be similar in magnitude to the difference between their azimuths. Thus if one of these problems is important in a particular situation it is likely that the other will be also. In the preceding section it was argued from a consideration of the equation of motion that τ_0 leads $\hat{U}$ in phase, which corresponds in the Ekman case to the azimuth of τ_0 being less than that of $\hat{U}$, and the direction of currents generally rotating clockwise with increasing height above the bed. This will be considered as the positive sense of

veering in what follows. With this analogy between the Ekman veering

problem and the Stokes shear wave problem the difference in azimuth between

τ_o and $\hat{U}$ can be obtained from Fig 15, where the parameter b becomes

$b_{Ek} = \left(\dfrac{2fh^2}{K}\right)^{1/2}$ for the Ekman case. The azimuth of $\hat{U}$ is 45° clockwise from

that of τ_o for infinitely deep water, reducing to 0° for water of zero

depth. b_{Ek} takes the value 0.94 using S-D Bank numerical values,

for which Fig 15 indicates the azimuth of $\hat{U}$ to be 1.7^o clockwise from that

of τ_o . A scale height can be defined as the height above the bed at

which the fractional departure from the free stream flow is $e^{-\pi}$,

$$Z_{Ek} = \pi \left(\frac{2K}{f}\right)^{1/2} \qquad\qquad - 17$$

A form for the steady boundary layer was derived without recourse to

artificial assumptions about an eddy viscosity distribution by Csanady

(1967) who postulated that near the bed a logarithmic velocity profile should

exist, while well away from the bed (in an infinitely deep flow) the profile

should obey a velocity defect law. Matching these profiles in an overlap

region yields an expression for the angle ψ between τ_o and the

geostrophic flow velocity, U_{∞}

$$\sin \psi = \frac{A}{k} \frac{u_*}{U_{\infty}} \qquad\qquad - 18$$

The value of A has to be determined experimentally. Using A = 5 (Tennekes,

1973) and S-D Bank values indicates that if the water depth were sufficiently

deep, and the flow steady, the total veering would be 38°. However, the

thickness of the boundary layer is shown by the same arguments to be Cu_*/f

which taking C = 0.3 (Tennekes, 1973) and S-D Bank values gives a boundary

layer thickness of 130m. In addition there should be no veering within

the logarithmic layer, so we would expect the total veering over the S-D

Bank to be very much less than in the idealised case.

An extension of Ekman's work to the case of an oscillatory stress was made
by Faller and Kaylor (1969) with boundary conditions appropriate to a wind-
induced surface current on an infinitely deep ocean with eddy viscosity
constant in space and time. A more sophisticated treatment was given by
Smith and Long (1976) who catered for driving forces of wind stress and/or
pressure gradient with any prescribed time dependence, and used an eddy
viscosity which increased linearly from the bed up to a chosen height and
was constant above this.

With neither treatment is it straightforward to obtain an estimate of
the veering for a particular set of conditions, especially as the veering
is now time-dependent, so estimates for the S- D Bank have not been made.

The two-layer model of Bowden et al (1959) discussed in the previous section
was applied to numerical values appropriate to Red Wharf Bay, and although
veering was not discussed it can be estimated from the results quoted.
At the time when the surface velocity is a maximum the veering between
surface and bottom amounts to 3.1^{o}, whilst when the surface velocity is
a minimum the veering is 60°. Shortly after slack water the veering
becomes slightly negative for a while.

The numerical model of Vager and Kagan (1969) discussed in the previous
section would be ideal for investigating the nature of veering under tidal
conditions, but unfortunately the authors give only a rather inadequate
discussion of results obtained from the model. The account given by
Weatherley (1975) of a very similar model applied to the Florida Current
gives a more thorough discussion of results, although, as discussed in the
previous section, these are not directly comparable to the S-D Bank
conditions. The time dependence of the total veering calculated by the
model is shown in Fig 25. It is interesting to note that the veering
becomes slightly negative shortly after slack water, as was found by

17

Bowden et al (1959).   A particularly important finding of this study was that although the logarithmic layer can be considered as quasi-steady the total Ekman layer was clearly not quasi-steady.

Field measurements of veering suffer from the limitation that most current meters give a much less precise reading of direction than of speed. Nevertheless a number of workers have performed experiments which can be interpreted in this way.   Weatherly (1972) made measurements in the Straits of Florida for comparison with his model, and unexpectedly found that there was 10.9° of veering between heights of 1m and 3m inside the logarithmic layer but effectively no turning above this, whereas his model predicted no veering inside the logarithmic layer but appreciable veering above it. Harvey and Vincent (1977) working in the southern North Sea found about 8° of veering between heights of 0.58m and 2.96m and about 6.5° of veering between 2.96m and 10m, indicating that veering was appreciable both within and above the logarithmic layer.   The measurements of Pingree and Griffiths (1974) on the edge of the continental shelf SW of Lands End show some scatter in the current directions, but the general indication is a veering of about 5° - 8° between heights of 2m and 98m.

Veering can be estimated from our own measurements of current speed and direction at heights of 0.5, 2, 4, 8 and 16m above the bed and 5m below the water surface at a site in Lyme Bay, 9km from the nearest coastline, where the water depth varied tidally from 29.5m to 37.5m and the bed was flat, horizontal and uniformly high rough.   The maximum current speed 5m below the surface was 104 cm s^{-1}.   Readings of direction were taken at each height every 30min over a period of 10.5 hours (with some gaps) and were the average of three spot readings, each with an accuracy of $\pm5^{\circ}$.   The direction reading at 5m below surface may possibly have been affected by the magnetic influence of the ship's hull.   The veering at each height was calculated relative to the direction at 0.5m.   As there

18
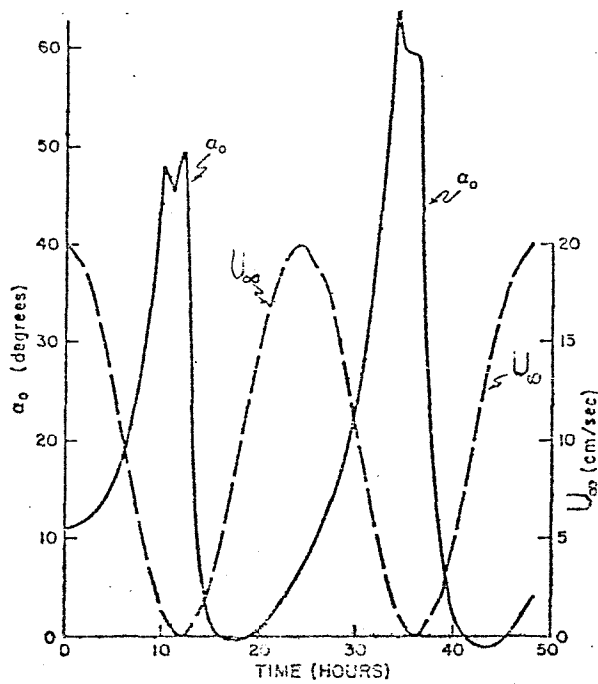
Fig 25.   The time-dependence of the total Ekman veering α_c (the angle
between the directions of U_∞ and $\mathcal{T}_\theta$) for Weatherly's (1975)
numerical model of the Florida Current. For reference the time-
dependence of U_∞ is shown.
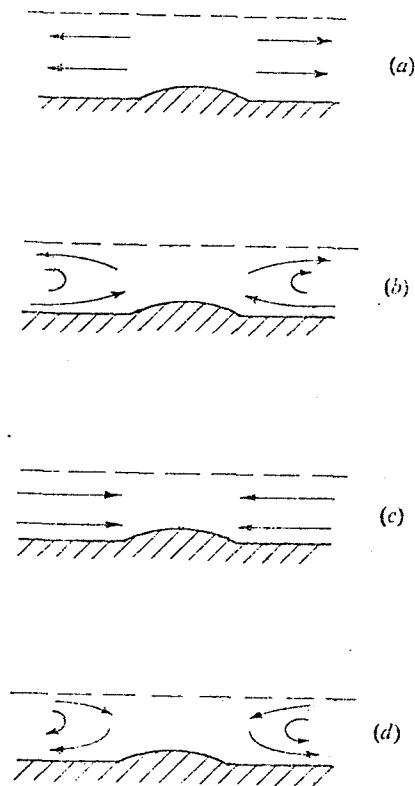
Fig 26.   Laminar secondary flow around the circular three-dimensional
hump modelled by Smith et al (1977) (a) upstream of the hump,
(b) on its forward face, (c) on the hump's leeward side, (d)
behind the hump.   The dashed line is associated with the modelling
technique.

was considerable scatter a meaningful measure could only be obtained by

calculating the mean veering at each height over the 10.5 hr period.

These, together with the standard errors are presented in Table 3.

| Height (m)	0.5	2	4	8	16	Surface -5
s.e.	-	1.6°	1.8°	3.6°	1.8°	7.5°
Mean veering	0°	-0.7°	0.7°	0.9°	2.4°	31°

Table 3. Veering relative to direction at 0.5m for Lyme Bay data.

The interpretation of a mean veering over a period of the order of a

tidal cycle is doubtful in view of the strong time-dependence shown in Fig. 22

but is the procedure adopted in all the field observations cited above.

Although the standard errors are large there is an indication that veering

in the correct sense occurs above about 8m, but is effectively zero below

that level. The thickness of the constant stress layer at this site

calculated as $0.2\,u_{*}^{2}/U_{x}f$ is 4.3m, so there is no turning within this

layer, as would be expected, nor within the next 4m, but appreciable turning

above this.

Finally the Marconi current meter data obtained to the west of the S-D Bank

(Fig 1) which was discussed in the previous section was checked for veering.

One hour at peak flood and one hour at peak ebb during the first tidal

cycle recorded were chosen, and the mean veering relative to the direction

at a height of 1.2m calculated. These angles, together with their

standard errors, are shown in Table 4.

Height (m)	1.2	3.2	4.2	6.2
s.e.(flood)	-	1.9°	0.6°	0.5°
Mean veering(flood)	0°	1.0°	2.1°	3.3°
s.e.(ebb)	-	1.4°	1.1°	1.3°
Mean veering (ebb)	0°	2.3°	3.1°	-2.4°

Table 4. Veering relative to direction at 1.2m for S-D Bank Marconi data.

Apart from the ebb value at 6.2m the veering is small, but in the correct sense.

Throughout this section it has been assumed that the sea and sea bed are horizontally homogeneous and of infinite horizontal extent. In practice the proximity of a coastline will confine the currents to run parallel to it, but it is not clear how far from the coast this effect will be felt.

In addition to Ekman veering the seabed topography may cause secondary flows which will cause the direction of $\mathcal{T}_o$ to be different to the direction of $\hat{U}$. This may be the cause of the negative veering observed in the S-D Bank area for the ebb tide. The main features of the secondary flow pattern in a two-dimensional laminar boundary layer encountering a three-dimensional lump are shown in Fig 2b, which was deduced from the theoretical flow field derived by Smith ~~and~~ et al (1977), though it is not clear to what extent this carries over to the case of a turbulent boundary layer. Secondary flow of this sort may well be of greater significance than Ekman veering in certain cases, but it will not be considered further because it is likely to be highly dependent on the particular topography and flow conditions, and hence hard to predict.

SPATIAL DEVELOPMENT OF THE BOUNDARY LAYER

It has been necessary to assume in most of the previous sections that the seabed is flat and uniform. If in fact the seabed is not flat, as in the case of the S-D Bank, both $\hat{U}$ and $\mathcal{T}_o$ must vary over the area and the relationship between them may also vary. We now examine this relationship, with an assumption that the flow is steady.

I am not aware of any studies of the present problem as such, so two indirect approaches have been used here. The first approach involves a review of

20

existing analytical, numerical and observational studies of flow over hills

and wavy surfaces, but the results of these studies must be applied

with caution to the S-D Bank situation, as most of the work assumes firstly

a deep flow for application to the atmosphere, and secondly two-dimensional

topography for ease of analysis.   A shallow flow over three-dimensional

topography behaves very differently to deep flow over two-dimensional

topography;   in the former case flow over the top of a bank will be slower

than the surrounding flow, because of the large drag in the shallow water,

whereas in the latter case it will be faster, to preserve continuity.

When two-dimensional continuity can be applied the fastest depth-averaged

flow will occur over the crests of the topography, so that if the position

of maximum shear stress can be located relative to the topography its

displacement from the maximum $\hat{U}$ is also known.   For an isolated hill

the displacement will be expressed as a fraction of the length L of the hill

measured between the points on the flanks at which the height is 1/10 the

crest height.   For sinusoidal topography the displacement is usually

expressed as a phase shift (generally a lead) of τ_{o} relative to $\hat{U}$

but for the present purposes it will also be interpreted as a fraction of L

where L is now the wavelength. L is roughly 6 km for the S-D Bank.

An analytical approach to deep flow over a two-dimensionally wavy boundary

was made by Benjamin (1959), who had to assume particular forms for the

velocity profile.   Using a turbulent-type velocity profile over a wavy

boundary he found that τ_{o} led $\hat{U}$ by 30° (.083 L).   He found the

same lead for a linear profile, whilst for a laminar-type profile he found a

lead of 60° (.17 L).   He generalises the linear profile case to flow over

an isolated hill of a specified shape and differentiation of his results

shows that the maximum stress occurs a distance .038 L upstream

of the crest.   A more recent study of deep turbulent flow over a two-

dimensional hill by Jackson and Hunt (1975) used an approach more in accord

with turbulence theory, though one of the assumptions he made is grossly

invalid in the S-D Bank case. As an example he quoted results for a hill of the same shape as that of Benjamin. Measured roughly from his diagram, the maximum τ_o occurred at a distance .016 L upstream of the crest. The problem of deep laminar flow over a three-dimensional hill was tackled analytically by Smith et al (1977). Their calculations of the distribution of longitudinal shear stress (for a differently shaped hill to Benjamin's are shown in Fig 27, from which the maximum shear stress is seen to lie a distance 0.13 L upstream of the crest. The same topography may of course give very different results in a turbulent flow. Two dimensional deep flow over almost sinusoidal sand waves was studied by Taylor and Dyer (1977) using numerical methods and a plausible turbulence closure. They found that the maximum stress occurred 19° (.053 L) upstream of the crest. Using similar techniques over an isolated hill Taylor (1977a,b) found that the maximum τ_o occurred a distance .053 L upstream of the crest.

Experimental work has also largely concentrated on flows which are two-dimensional and many times deeper than the height of the topography. Zilker et al (1977) made measurements over a wavy boundary of steepness .0125 in fully developed turbulent channel flow and found that the maximum was located 51° (.14 L) upstream of the crest. Similar work was performed by Smith (1969) over a pair of sinusoidal waves of steepness .067 in a flume, with water depths of 7.5 and 6.3 times the wave height. In the first case the first harmonic of the τ_o distribution had a phase lead of 45° (.13 L) relative to the bedform, whilst in the second case the lead was 32° (.089 L). Velocity profiles and bed shear stresses are tabulated in Smith's report, so that it would be possible, though time-consuming, to calculate both τ_o and $\hat{U}$ over the waves.

Smith (1969) also made field measurements over a sandwave of height about 3m and length 80m in the Columbia River, USA, with a water depth of 12m
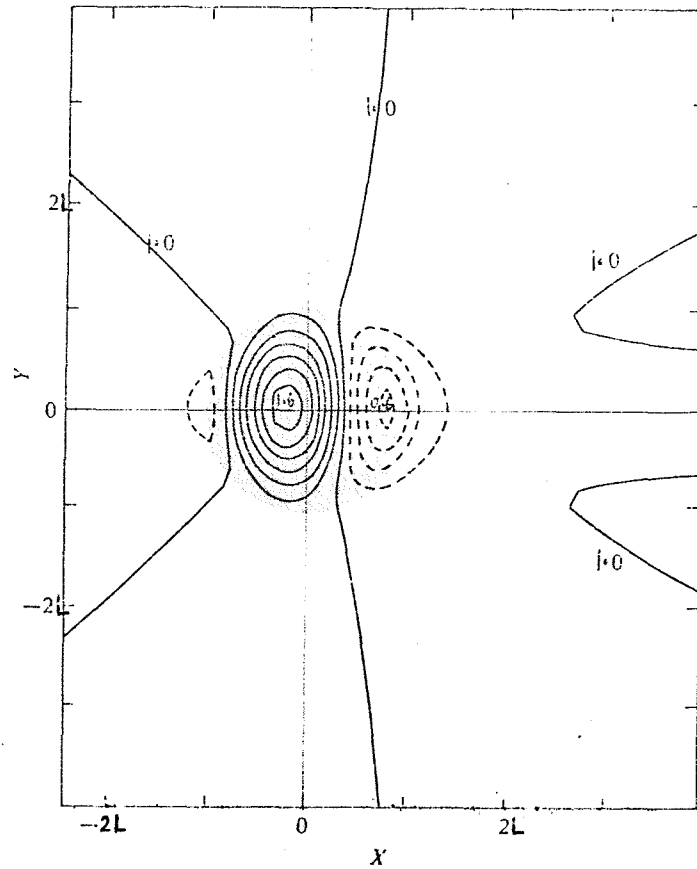
Fig 27.   Contours of constant longitudinal shear stress relative to the
           free-stream value for laminar flow around the circular three-
           dimensional hump modelled by Smith et al (1977).   Solid lines
           indicate values greater than unity, dotted lines indicate values
           less than unity, the contour interval is 0.1, and the position
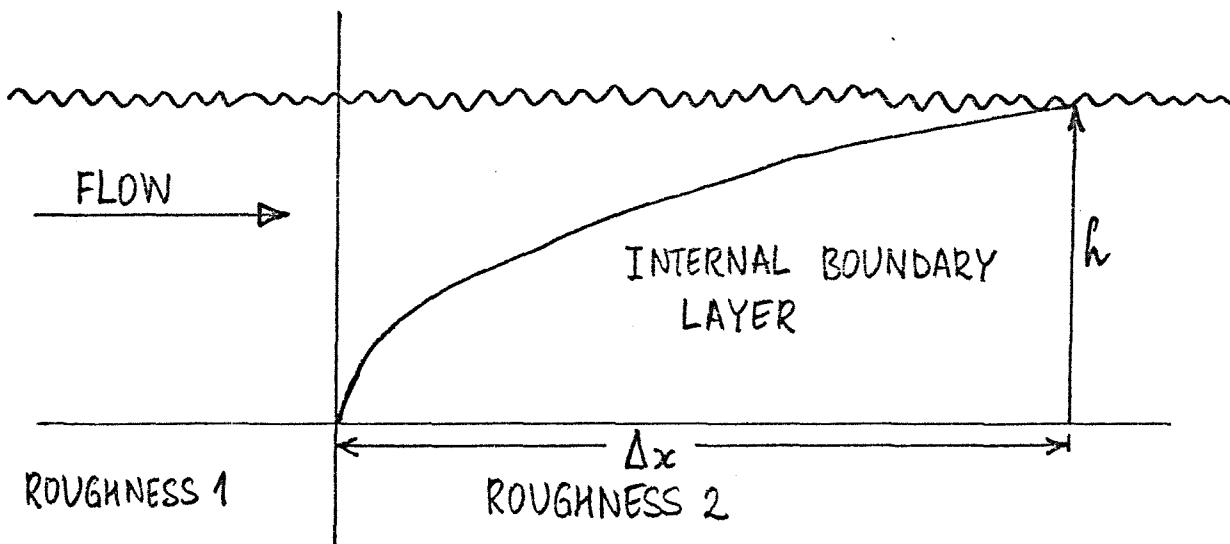   of the hump is shaded.

Fig 28.   Schematic diagram of the growth of an internal boundary layer
           downstream of an abrupt change in surface roughness.

over the crest. The shape of the sandwave departs sufficiently from
sinusoidal that it is not possible to attribute a phase to τ_c. Smith performs
a harmonic analysis of the shape of the wave, and from this synthesises
a predicted shear stress distribution using his own theory which gives
good agreement with the measured shear stress distribution. He also
presents velocity profiles over the wave, which clearly show that the
profile is not locally adjusted over topography of this scale. Field
measurements have also been made by Dyer (1970) over a sandwave. The
measurements of τ_c cannot be interpreted in terms of phase as they exhibit
scatter due to the presence of smaller bed features and in addition the mean
stream velocity was varying tidally during the experiment. However it is
again clear that the profiles vary considerably in shape over the wave,
and are not locally adjusted.

The second approach to the problem is to consider adjustment of the
boundary layer over topography by analogy with the adjustment downstream
of an abrupt change of surface roughness. This may give some feel for
the topography problem, although the two problems do have distinct
differences. It is found experimentally that downstream of a roughness
change the surface shear stress adjusts rapidly to its new value (Bradley,
1968) while an internal boundary layer forms, thickening slowly until at a
distance Δx downstream the new profile is fully adjusted (Fig 28). Thus
an estimate of τ_c shortly after the roughness change should be related
to the profile, and hence $\hat{U}$, at a point Δx downstream. The
varying topography can be interpreted as continuously varying surface conditions,
in this case surface displacement, which the boundary layer is continuously
adjusting to, so that τ_c should everywhere be associated with $\hat{U}$ at a
distance Δx downstream, with Δx a function of position. To first order
the error $\Delta \tau_c$ made in calculating τ_c from the local $\hat{U}$ will be

$$\Delta \tau_c = - \Delta x \frac{d\tau_c}{dx}$$

- 19

23

Since $d\tau_0/dx$ can be roughly calculated from the present model results
for the S-D Bank, an order of magnitude estimate of $\Delta\tau_0$ can be made
provided Δx can be estimated.

A time-scale for development of the logarithmic part of the velocity profile
is given by Z_i / U_* where Z_i is the height of the log layer. A
disturbance in the log layer will be advected downstream at a velocity close
to $\hat{U}$, so that a spatial scale for adjustment is given by $Z_i \hat{U}/U_*$.
If the water depth h is sufficiently shallow these arguments can be
extended to the entire boundary layer, giving a crude estimate of Δx as

$$\Delta x = \frac{h\,\hat{U}}{U_*} = h \cdot C_f^{-1/2} \qquad\qquad - 20$$

Fitting S-D Bank values gives $\Delta x \sim 200\,m$.

A more rigorous argument is given by Miyake in an unpublished thesis
quoted by Busch (1973), who proposes that the rate of increase of Z_i
is proportional to U_* where Z_i is now the height of the interface between
the 'old' flow and the internal boundary-layer, so that

$$\bar{U} \frac{dz_i}{dx} = B\,U_* \qquad\qquad -21$$

where B is a constant, and $\bar{U}$ the mean velocity at height Z_i .
Substituting a logarithmic velocity profile for $\bar{U}$ and integrating gives

$$\Delta x = \frac{Z_i}{A} \left(\ln \frac{Z_i}{Z_0} - C \right) \qquad\qquad - 22$$

The values of the constants A and C determined from field and laboratory
experiments over a roughness change are given variously by Busch (1973)
as $A = 0.6, C = 1$; by Jackson (1976) as $A = 0.3, C = 0.65$; and by
Mulhearn (1977) as $A = 0.32, K = 1$. Jackson (1976) showed that the best

24

fit is obtained if the value of z_o taken is that for the rougher

surface, and his values of the constants A and C will be used here.

The logarithmic velocity profile can be extended to the water surface

without too much error so that $Z_i = h$. Then as $\hat{U} \simeq \bar{U}(h)$

we have approximately

$$\Delta x = \frac{h}{0.3} \left(k \, C_f^{-1/2} - 0.65 \right)$$

-23

This is the distance downstream at which the interface reaches the

surface, and is the distance we will use, though the boundary layer does not

completely reach equilibrium until many times this distance downstream.

Fitting S-D Bank values gives $\Delta x = 245\,m$. This is consistent with

the estimates obtained by the first approach in which the maximum of τ_o was

found to be located upstream of the maximum $\hat{U}$ by a distance variously

estimated as between $.016\,L$ and $0.14\,L$, corresponding to 96m to 840m

for the S-D Bank.

The numerical model predicts the value of τ_c at gridpoint 106 (Fig 1)

at the maximum flood velocity to be 28.5 dynes cm^{-2}, while at a position

200m south the predicted value is 30.3 dynes cm^{-2}. The flood current is

approximately south going, so that $d\tau_o/dx$ can be calculated from these

figures and inserted in Eq 19, together with the value of Δx found above

to give $\Delta \tau_c = -2.2$ dynes cm^{-2}. This represents a 7% error in the

stress, which should be about the largest error found in the S-D Bank area

as gridpoint 106 has one of the steepest along-tide bed gradients.

Around the S-D Bank there are additionally variations of bed roughness

associated with the various types of bottom sediment. The arguments

given above can equally be applied at a change in bed roughness, and with

greater rigour.

It has been assumed throughout this section that the flow does not separate

in the lee of the sandbank. Taylor and Dyer (1977) have reviewed the

experimental evidence for separation in the lee of sandwaves, and found that

a most conservative criterion is that the wave steepness needs to exceed .05,

while some workers failed to obtain separation at a steepness of 0.1. As

the steepness at gridpoint 106 is only .01 it is very unlikely that

separation occurs.

IMPLICATIONS FOR SEDIMENT TRANSPORT

The values of τ_o predicted by the S-D Bank model will ultimately be

applied to sediment transport formulae, so it is important to know what

error in sediment transport rate will result from a given error in τ_o

Considering bedload transport first, Smith (1969) found that one of the more

reliable formulae was that due to Yalin (1963). When τ_o is much greater

than the threshold bed shear stress τ_c this expression for bedload trans-

port rate q_b reduces to

$$q_b = 0.635 \left(\rho_s - \rho \right) d\, \tau_o^{1/2} \left(\tau_o - \tau_c \right) / \tau_c \qquad - 24$$

where ρ_s is the density and d the diameter of the sediment grains, and

ρ is the density of water. A fractional error in τ_o will cause a larger

fractional error in $\left(\tau_o - \tau_c \right)$ so that a 10% error in τ_o would lead

to an error in q_b which is greater than 15%. When τ_o is only

slightly greater than τ_c the full expression reduces to

$$q_b = 0.778 \left(\frac{\rho}{\rho_s} \right)^{0.4} \left[\frac{(\rho_s - \rho)d}{g} \right]^{1/2} \tau_o^{1/2} \left(\tau_o - \tau_c \right)^2 / \tau_c^{3/2} \qquad - 25$$

where g is the acceleration due to gravity. In this case a 10% error

in τ_o would lead to an error in q_b which is greater than 25%.

A suitable criterion for suspension adapted from the ideas of Bagnold (1966)

is that the ratio $W_s / K u_*< 6$ where W_s is the settling velocity of the grains

and $K \sim 0.4$ is von Karman's constant. Using S-D Bank values of $u_* = 5$ with

26

a grain diameter of $180 \mu m$ gives $W_s/\kappa u_* = 1.5$ so suspension is clearly important. The diffusion equation for the mass concentration of sediment under steady horizontally homogeneous conditions reduces to

$$W_s C = - K_s \frac{dC}{dz}$$

- 26

where K_s is the eddy diffusion coefficient.

The eddy viscosity coefficient takes the form $K = \kappa u_* z$ in the lowest portion of the flow, and provided most of the sediment is confined to this portion it can be assumed that $K_s = K = \kappa u_* z$ throughout the full depth, as departures from this form higher in the flow will not significantly affect the sediment. Inserting this in Eq 26 and integrating from a reference height z_a to the water surface $z = h$ gives

$$\frac{C(z)}{C(z_a)} = \left(\frac{z}{z_a}\right)^{-b} \quad \text{with} \quad b = \frac{W_s}{\kappa u_*}$$

- 27

The assumption made will generally be valid if b is sufficiently large, as will frequently be the case for sand grains in the sea, under which conditions the form $K_s = \kappa u_* z \frac{(h-z)}{h}$ used by Rouse (1937) in deriving his well known concentration profile is unnecessarily complicated. In the lowest part of the flow the velocity profile is logarithmic, so that if the reference height is identified with z_0 the suspended sediment transport rate is

$$q_s = \rho \int_{z_0}^{h} C(z) U(z) \, dz$$

$$= \rho \int_{z_0}^{h} C(z_0) \left(\frac{z}{z_0}\right)^{-b} \frac{u_*}{\kappa} \ln\left(\frac{z}{z_0}\right) dz$$

$$= \frac{\rho C(z_0) u_* z_0}{\kappa (1-b)^2} \left\{ \left(\frac{h}{z_0}\right)^{1-b} \left[\ln\left(\frac{h}{z_0}\right) - b \ln\left(\frac{h}{z_0}\right) \right] + 1 \right\}$$

- 28

A little work shows that if in addition

$$b > 1 + \frac{6.64}{\ln(h/z_0)}$$

- 29

then the expression in curly brackets is equal to unity to an accuracy better than 1%, so that

$$q_s = \rho \frac{C(z_0) \, U_* Z_0}{k \, (1-b)^2} \qquad - 30$$

Smith and McLean (1977) find that the reference concentration is well represented by

$$C(z_0) = \gamma_1 \frac{(\tau_0 - \tau_c)}{\tau_c} \left(\frac{\rho_s}{\rho}\right) \qquad - 31$$

provided the excess shear stress is not too large, where γ_1 is experimentally found to take the value 1.24×10^{-3}. Thus

$$q_s = \frac{k \, \gamma_1 \, \rho_s \, U_*^3 \, Z_0}{(k U_* - W_s)^2} \frac{(\rho U_*^2 - \tau_c)}{\tau_c} \qquad - 32$$

This expression shows the dependence of q_s on U_* more clearly than does Einstein's (1950) which cannot be presented analytically as he used the Rouse concentration profile which makes the integration impossible in closed form. The two expressions give almost identical results within the range of conditions which satisfy the assumptions made here.

On top of the S-D Bank the sand is likely to be rippled, so that Z_c might be expected to take a value of about 0.5cm, and in addition a proportion of the measured value of τ_0 will be due to the spatially averaged form drag over the ripples. The proportion is often taken as 0.5, so that the maximum value of U_* due to skin friction is 3.54 cm s^{-1} corresponding to $\tau_0 = 25$ dynes cm^{-2}, which taken together with $W_s = 3$ cm s^{-1} and $\tau_c = 2$ dynes cm^{-2}, corresponding to 180 μm grains, and $h = 5m$ gives $b = 2.119$ and $1 + 6.64/\ln(h/z_0) = 1.96$. Thus condition 29 is satisfied and q_s is given by Eq 32 as 0.0615 gm cm^{-1}s^{-1}. If τ_0 is increased by 10% and the other values remain the same, Eq 32 gives $q_s = 0.0859$ gm cm^{-1}s^{-1}, corresponding to a change of 40%.

There are at present still serious shortcomings in the applicability of sediment transport formulae in general. One of these is the problem

28

referred to above of identifying the contribution to τ_o due to form drag on ripples and larger features, which plays no part in moving the sediment. This has been examined by Smith and McLean (1977) who showed that the skin friction velocity U_{*0} over ripples of height H and wavelength λ is related to U_{*1} measured at a height much greater than H by

$$ \frac{U_{*1}}{U_{*0}} = \left\{ 1 + \frac{C_b}{2\kappa^2} \frac{H}{\lambda} \left[\ln a_1 \left(\frac{\lambda}{z_0} \right)^{0.8} \right]^2 \right\}^{1/2} \qquad - 33 $$

where a_1 is a constant and C_b is a drag coefficient for the ripple. Typical figures for the S-D Bank can be guessed as H = 3cm, λ = 20cm, z_0 = .05cm due to grains alone using the value for the area of the Marconi current measurements assuming it was unrippled; and using Smith and McLean's experimental values of a_1 = 0.1 and C_D = 0.2 assuming the flow separates over the ripples gives

$$ \rho U_{*0}^2 = 0.63 \rho U_{*1}^2 \qquad - 34 $$

in comparison with the commonly used figure of 0.5 taken above. Smith (1977) acknowledges that this is still a contentious area, and it is likely that errors in the estimation of ρU_{*0}^2 well in excess of $\pm$ 10% can be attributed to this cause.

He also identifies three other major grey areas in the applicability of sediment transport formulae. Expressions for the reference concentration $C(z_0)$ have been given by a few workers, but these give widely differing answers. This subject has not been given the attention it warrants either theoretically or experimentally and represents a serious source of error. The non-linear relationship between sediment transport rate and τ_c means that an average value of τ_c will give misleading results when used to estimate sediment transport in naturally occurring situations where τ_o is highly intermittent in both space and time. Lastly there is such a

dearth of field measurements of marine sediment transport that none
of the available sediment transport theories can be considered as
thoroughly tested.

30

SUMMARY, DISCUSSION AND CONCLUSIONS

The relationship between the bed shear stress τ_c and the depth averaged flow velocity $\hat{U}$ has been examined in terms of differences of (i) phase of the tidal cycle, (ii) direction, and (iii) spatial distribution, with particular application to conditions in the Sizewell-Dunwich (S-D) Bank area.

(i) Analytical and numerical models of oscillatory flow over a flat bed (Table 5) show that when the water is sufficiently deep τ_c leads $\hat{U}$ by a phase variously estimated at between 8° and 45°. In shallower depths comparable to those around the S-D Bank, however, this predicted phase lead reduces to 1.6° to 1.9°, corresponding to $3.2 - 3.8$ mins. Field observations in depths both comparable with and very much deeper than those around the S-D Bank generally indicate τ_c leading $\hat{U}$ by between 9° and 13°, corresponding to 18-26 mins, although some cases have been reported of τ_c lagging $\hat{U}$. Analysis of current measurements made in the S-D Bank area shows a complicated picture with τ_c leading $\hat{U}$ at times of maximum flow, but τ_c lagging $\hat{U}$ when velocities are smaller. The drag coefficient $C_f = \tau_c / \hat{U}^2$ varies considerably through a tidal cycle. In areas of mobile sand the changing ripple pattern will also cause C_f to vary and further complicate matters.

(ii) Under conditions of deep steady flow in the northern hemisphere analytical models of Ekman veering (Table 6) show that the azimuth of τ_c is less than that of $\hat{U}$ by an angle variously estimated as 38° to 45°. In shallower depths comparable to those around the S-D Bank this reduces to 1.7°. When the flow is time-dependent the veering is also time-dependent; for a tidal flow in shallow water the veering at the time of maximum flow is variously predicted to be between 3.1° and 6°, though at minimum flow this increases to 59° to 69°. The time dependence makes the interpretation of field observations of veering difficult, because estimates have usually been averaged over a tidal cycle. Observations made in both deep and shallow water generally indicate mean veering of $5^\circ - 15^\circ$. Analysis of current measurements in the S-D Bank area at time of maximum flow show veering in the lowest 6.2m of up to 3.3°. An anomolous value of -2.4° in this area may be attributable to secondary flows associated with the bank. These may be as important a factor in determining the direction of τ_c relative to that of $\hat{U}$ as Ekman veering, though more difficult to estimate.

(iii) The flow of shallow water over three-dimensional topography does not

appear to have been systematically studied either analytically, numerically
or experimentally, so that two indirect approaches have been used here.
Analytical and numerical work on deep flow over two-dimensional waves and hills
(Table 7) indicates that the maximum τ_o occurs upstream of the maximum
$\hat{U}$ by a distance estimated variously as between .016L and .13L, where L
is the length of the hill or the wavelength of the wave. Laboratory experiments
over a wavy boundary give values between .089L and .14L. .016L represents
96m in terms of the S-D Bank, and .14L represents 840 m. Field observations
in the literature are not easily interpreted in these terms.

The second approach is an analogy with the flow development downstream
of an abrupt change in surface roughness. The interface of the internal
boundary layer which grow downstream of the roughness change reaches the water
surface at a distance 245m downstream of the change, using S-D Bank numerical
values. This displacement of τ_o from $\hat{U}$ can be interpreted as leading to
a 7% error in the estimation of τ_o at the northern edge of the bank. There
will additionally be similar displacements at the boundaries between zones of
different bed roughness in the area. The flow is unlikely to separate in the
lee of the bank.

The value of τ_o obtained from the model represents the sum of the skin
friction acting on the sand grains and the spatially averaged form drag of the
ripples and possibly larger bedforms. The skin friction, needed for insertion
into sediment transport formulae, can only be estimated at present by assuming
an arbitrary partition of the total bed shear stress. The bedload transport
rate is proportional to $\tau_o^{1/2} \left(\tau_o - \tau_c \right)$ at high transport rates, where
τ_c is the threshold shear stress, so that a 10% error in τ_o leads to an
error in the transport rate which is greater than 15%. At low transport rates
the error becomes greater than 25%. The maximum shear stress over the S-D
Bank is many times the threshold stress, so that it is likely that suspension
is the dominant mode of transport. A plausible form of equation for the
suspended load indicates that a 10% error in τ_o leads to a 40% error in the
suspended sediment transport rate in conditions typical of the S-D Bank.

The primary effect of a simple phase lead of τ_o relative to $\hat{U}$ is
to cause a shift in the time at which sediment moves, but not in the quantity,
so that averaged over a tidal cycle the net transport is unchanged. Thus only
second order effects, such as the introduction of higher harmonics in τ_o ,
the modification of the model's prediction of $\hat{U}$, and the need for a non-
stationary sediment transport formula, are felt. As the phase lead is likely
to be only a few degrees in the S-D Bank case, omitting it will probably not
introduce a serious error into sediment transport calculations. Ekman veering

Author	Phase by which τ_c leads $\hat{U}$	Comments
Analytical Models		
Lamb (1975)	45°	Deep water
after Lamb (1975)	1.9°	For S-D Bank values
Smith (1977)	8°	Deep water
Bowden et al (1959)	1.6°	Shallow water
Numerical Models		
Valer & Kagan (1969)	20°	Deep water
Weatherly (1975)	26°	Deep water
Field Observations		
Weisberg and Sturges (1976)	9° to 13°	Shallow estuary
Pingree and Griffiths (1974)	13°	Deep water
Gordon (1975)	-29°	Shallow estuary
IOS(T)	10°	Weymouth Bay - fairly shallow
IOS(T)	Variable	S-D Bank area

TABLE 5   Phase lead of τ_c relative to $\hat{U}$.   In some of the examples phases which were cited for near-bottom currents have been identified here with τ_c , and similarly currents well away from the bottom have been identified with $\hat{U}$.

Author	Angle by which τ_o is anticlockwise of $\hat{U}$	Comments
Analytical Models		
Ekman (1905)	45°	Steady flow, deep water
Csanady (1967)	38°	Steady flow, deep water
after Ekman (1905)	1.7°	Steady flow, S-D Bank values
Bowden et al (1959)	3.1°	Oscillatory flow, max velocity, shallow water
" " "	69°	Oscillatory flow, min velocity, shallow water
Numerical Model		
Weatherly (1975)	6°	Oscillatory flow, max velocity, deep water
" "	59°	Oscillatory flow, min velocity, deep water
Field Observations		
Weatherly (1972)	10.9°	Deep water
Pingree and Griffiths (1974)	5° to 8°	Deep water
Harvey and Vincent (1977)	14.5°	Fairly shallow water
IOS(T)	2.4°(to 31°?)	Lyme Bay - fairly shallow
IOS(T)	3.3°(-2.4°?)	S-D Bank area

TABLE 6   Veering of τ_o relative to $\hat{U}$.   As in Table 5 near-bottom currents have been identified with τ_o and currents away from the bed identified with $\hat{U}$.

Author	Distance max. τ_o is upstream of max $\hat{U}$	Topography	Comments
Analytical models			
Benjamin (1959)	.083L	Waves	Deep 2-D flow
" "	.038L	Hill	" " "
Jackson and Hunt (1975)	.016L	Hill	Deep 2-D flow
Smith et al (1977)	.13L	Hill	Deep 3-D laminar flow
Numerical Models			
Taylor and Dyer (1977)	.053L	Waves	Deep 2-D flow
Taylor (1977 a,b)	.053L	Hill	Deep 2-D flow
Laboratory Experiments			
Zilker (1977)	.14L	Waves	2-D flow
Smith (1969)	.089L to .13L	Waves	Fairly shallow 2-D flow

TABLE 7   Spatial displacement of τ_o relative to $\hat{U}$. L represents the wavelength in the waves examples, and the distance between the points at which the height is 1/10 the crest height in the hill examples.

between τ_c and $\hat{U}$ will cause a small eastwards component of sediment transport across the bank on a flood tide and a similar westward component on an ebb tide. The difference in direction amounts to only a few degrees in the S-D Bank case, so its omission is also unlikely to seriously affect sediment transport calculations. Displacement of τ_c relative to $\hat{U}$ due to spatial development of the boundary layer over the bank will result in increased erosion on the upstream flank and decreased erosion on the downstream flank. The displacement in the S-D Bank case is equivalent to a little more than one grid space of the model so that it may well be appreciable, and the 7% error in τ_c thus caused will produce an error of roughly 28% in the suspended sediment transport rate. These latter results, which were inferred from considerations of deep flow over two-dimensional topography, are sufficiently significant to indicate the need for further studies of the more realistic case of shallow flow over three-dimensional topography.

Suppose that the best available three-dimensional model were used instead of the present vertically-integrated model. We might expect better (though still imperfect) prediction of the tidal variation of the magnitude and direction of τ_c , and of its topographically induced variation including secondary flow effects. However, the precision obtained in τ_c would be out of all proportion to the accuracy of the sediment transport formulae with which it would be used. Major gaps in the applicability of sediment transport formulae include the partition of τ_c into form drag over bedforms and skin friction acting on the sediment, the calculation of the suspended sediment concentration at a reference level, the treatment of non-uniformity effects in space and time, and the testing of the formulae under field conditions. The error introduced by any one of the above weak points in the sediment transport theory is likely to outweigh the errors introduced by the prediction of τ_o using the vertically integrated model.

Thus the numerical model should continue to be developed as at present, while further work should concurrently be done on the following topics:
(i) Calculation of τ_o and $\hat{U}$ from the laboratory velocity profiles over a wavy bottom tabulated by Smith (1969) to give a direct intercomparison of the two.
(ii) The development, possibly by Dr B Johns of the University of Reading, of a three-dimensional numerical model of shallow flow over topography of some idealised shape.
(iii) Adaptation of Smith's (1977) analytical model of oscillatory flow over a flat bottom to the case of finite water depth to give a reasonable estimate of the phase lead of τ_o relative to $\hat{U}$ in the S-D Bank case.

(iv) Development of a high-order closure numerical model of oscillating flow over a flat bottom including Coriolis effects, as detailed by Vager and Kagan (1969) and Weatherly (1975). Apart from giving accurate predictions of the tidal dependence of the magnitude and direction of τ_o in the S-D Bank area, this will give insight into the behaviour of the tide on the continental shelf in general, in particular the temporal and spatial distribution of the boundary layer.

(v)   Further analysis of the Marconi current meter data. A method similar to that used by Pingree and Griffiths (1974) would be the most generally useful.

(vi) Analysis of the Braystoke current meter measurements made at three positions on the bank once the data is in a usable form, using the method above.

(vii) Determination of the distribution of C_f and z_o over the whole S-D Bank area by making measurements similar to those above.

REFERENCES

BAGNOLD, R.A. 1966.   An approach to the sediment transport problem from
        general physics.   Geological Survey Professional Paper 422-I.
        US Govt. Printing Office, Washington.

BENJAMIN, T.B. 1959.   Shearing flow over a wavy boundary. Journal of Fluid
        Mechanics, 6(2), 161-205.

BOWDEN, K.F., L.A. FAIRBAIRN and P. HUGHES, 1959.   The distribution of
        shearing stresses in a tidal current. Geophysical Journal of the
        Royal Astronomical Society, 2, 288-305.

BRADLEY, E.F. 1969.   A micrometeorological study of velocity profiles and
        surface drag in the region modified by a change in surface
        roughness, Quarterly Journal of the Royal Meteorological Society,
        94, 361-379.

BUSCH, N.E. 1973.   On the mechanics of atmospheric turbulence.   Workshop on
        Micrometeorology, Ed. by D.Haugen, Americal Meteorological Society,
        1 - 65.

CHANNON, R.D. and D. HAMILTON, 1971.   Sea Bottom Velocity Profiles on the
        continental shelf south-west of England.   Nature, 231, 383-385.

CSANADY, G.T. 1967.   On the 'resistance law' of a turbulent Ekman layer.
        Journal of the Atmospheric Sciences, 24, 467 - 471.

DAVIES, A.G. 1977.   A mathematical model of sediment in suspension in a
        uniform reversing tidal flow.   Geophysical Journal of the Royal
        Astronomical Society, 51, 503 - 529.

DYER, K.R. 1970.   Current velocity profiles in a tidal channel.   Geophysical
        Journal of the Royal Astronomical Society, 22, 153 - 161.

EINSTEIN, H.A. 1950.   The bed-load function for sediment transportation in
        open channel flows. U.S. Department of Agriculture Technical
        Bulletin no. 1026, 71 pp.

EKMAN, V.W. 1905.   On the influence of the earth's rotation on ocean
        currents.   Arkiv foer Matematik, Astronomi och Fysik, 2(11),1-53.

FALLER, A.J. and R. KAYLOR 1969.   Oscillatory and transitory Ekman boundary
        layers. Deep Sea Research, Supplement to Vol. 16, 45-58.

GORDON, C.M. 1975.   Sediment entrainment and suspension in a turbulent tidal
        flow.   Marine Geology, 18, M57-M64.

HARVEY, J.G. and C.E.VINCENT 1977.   Observations of shear in near-bed currents
        in the southern North Sea.   Estuarine and Coastal Marine Science,
        5, 715-731.

JACKSON, N.A. 1976.   The propagation of modified flow downstream of a change in
        roughness. Quarterly Journal of the Royal Meteorological Society,
        102, 775-779.

JACKSON, P.S. and J.C.R. HUNT, 1975. Turbulent wind flow over a low hill. Quarterly Journal of the Royal Meteorological Society, 101, 929 - 955.

JOHNS, B. 1969. Some consequences of an inertia of turbulence in a tidal Estuary. Geophysical Journal of the Royal Astronomical Society, 18, 65 - 72.

JOHNS, B. 1970. On the determination of the tidal structure and residual current system in a narrow channel. Geophysical Journal of the Royal Astronomical Society, 20, 159 - 175.

JOHNS, B. 1975. The form of the velocity profile in a turbulent shear wave boundary layer. Journal of Geophysical Research, 80 (36), 5109 - 5112.

JOHNS, B. 1976. A note on the boundary layer at the floor of a tidal channel. Dynamics of Atmospheres and Oceans, 1, 91 - 98.

JOHNS, B. 1977. Residual flow and boundary shear stress in the turbulent bottom layer beneath waves. Journal of Physical Oceanography, 7, 733 - 738.

LAMB, H. 1975. Hydrodynamics (6th Edition). Cambridge University Press, 738 pp.

LEES, B.J. 1977. Sizewell-Dunwich Bank Project. Institute of Oceanographic Sciences Report no. 38, 15 pp.

MONIN, A.S. and A.M.YAGLOM. 1971. Statistical fluid mechanics, Vol.1. MIT Press, 769 pp.

MULHEARN, P.J. 1977. Relations between surface fluxes and mean profiles of velocity, temperature and concentration, downwind of a change in surface roughness. Quarterly Journal of the Royal Meteorological Society, 103, 785 - 802.

PINGREE, R.D. and D.K.GRIFFITHS, 1974. The turbulent boundary layer on the continental shelf. Nature, 250, 720 - 722.

ROUSE, H. 1937. Modern conceptions of the mechanics of turbulence. Transactions of the American Society of Civil Engineers, 102, 463 - 543.

SMITH, F.T., R.I.SYKES and P.W.M.BRIGHTON. 1977. A two-dimensional boundary layer encountering a three-dimensional hump. Journal of Fluid Mechanics, 83 (1), 163 - 176.

SMITH, J.D. 1969. Investigations of turbulent boundary layer and sediment-transport phenomena as related to shallow marine environments, no. A69:7, Department of Oceanography, University of Washington, 69 pp.

SMITH, J.D. 1977.   Modelling of Sediment Transport on Continental Shelves.
The Sea , Vol.6, Ed. by E.D.Goldberg.   Wiley-Interscience,
539 - 577.

SMITH, J.D. and C.E. LONG. 1976.   The effect of turning in the bottom boundary
layer on continental shelf sediment transport. Mémoires Société
Royale des Sciences de Liège, 6e série, 10, 369-396.

SMITH, J.E. and S.R.McLEAN, 1977.   Spatially averaged flow over a wavy surface.
Journal of Geophysical Research, 82 (12),   1735 - 1746.

TAYLOR, P.A. 1977a.   Some numerical studies of surface boundary-layer flow
above gentle topography.   Boundary-Layer Meteorology, 11,
439 - 465.

TAYLOR, P.A. 1977b.   Numerical studies of neutrally stratified boundary-layer
flow above gentle topography. I: Two-dimensional cases. Boundary -
layer Meteorology, 12, 37 - 60.

TAYLOR, P.A. and K.R.DYER 1977.   Theoretical models of flow near the bed and
their implications for sediment transport.   The Sea , Vol.6,
Ed. by E.D.Goldberg, Wiley-Interscience, 579 - 601.

TENNEKES, H. 1973.   Similarity Laws and scale relations in planetary boundary
layers.   Workshop on Micrometeorology. Ed. by D. Haugen, American
Meteorological Society, 177 - 216.

THORN, M.F.C. 1975.   Hysteresis of fine sand suspensions in a tidal estuary.
Hydraulics Research Station Notes, 17, 2 - 3.

VAGER, B.G. and B.A.KAGAN. 1969.   The dynamics of the turbulent boundary layer
in a tidal current.   Izvestiya Atmospheric and Oceanic Physics,
5 (2), 88 - 93.

WEATHERLY, G.L. 1972.   A study of the bottom boundary layer of the Florida
Current. Journal of Physical Oceanography, 2, 54 - 72.

WEATHERLY, G.L. 1975.   A numerical study of time-dependent turbulent Ekman
layers over horizontal and sloping bottoms.   Journal of Physical
Oceanography, 5, 288 - 299.

WEISBERG, R.H. and W. STURGES. 1976.   Velocity observations in the West
Passage of Narragansett Bay: a partially mixed estuary.   Journal
of Physical Oceanography, 6, 345 - 354.

WIMBUSH, M. and W. MUNK. 1970.   The benthic boundary layer. The Sea , Vol.4
Part 1, Ed. by A.E.Maxwell, Wiley-Interscience, 731 - 758.

YALIN, M.S. 1963.   Mechanics of sediment transport.   Pergamon Press, 290 pp.

ZILKER, D.P., G.N.COOK and T.J.HANRATTY, 1977.   Influence of the amplitude
of a solid wavy wall on a turbulent flow.   Part 1. Non-separated
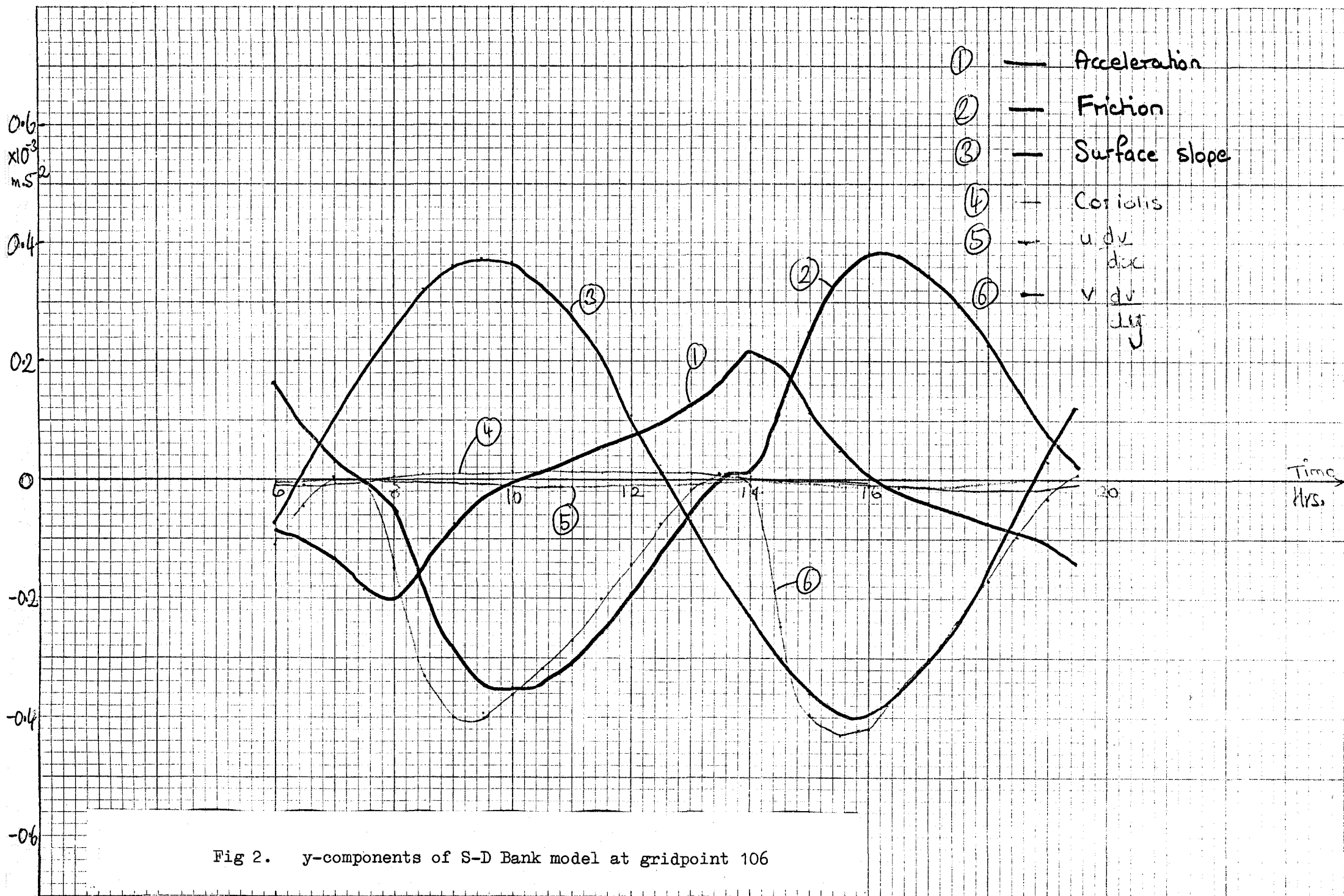flows.   Journal of Fluid Mechanics, 82(1), 29 - 51.

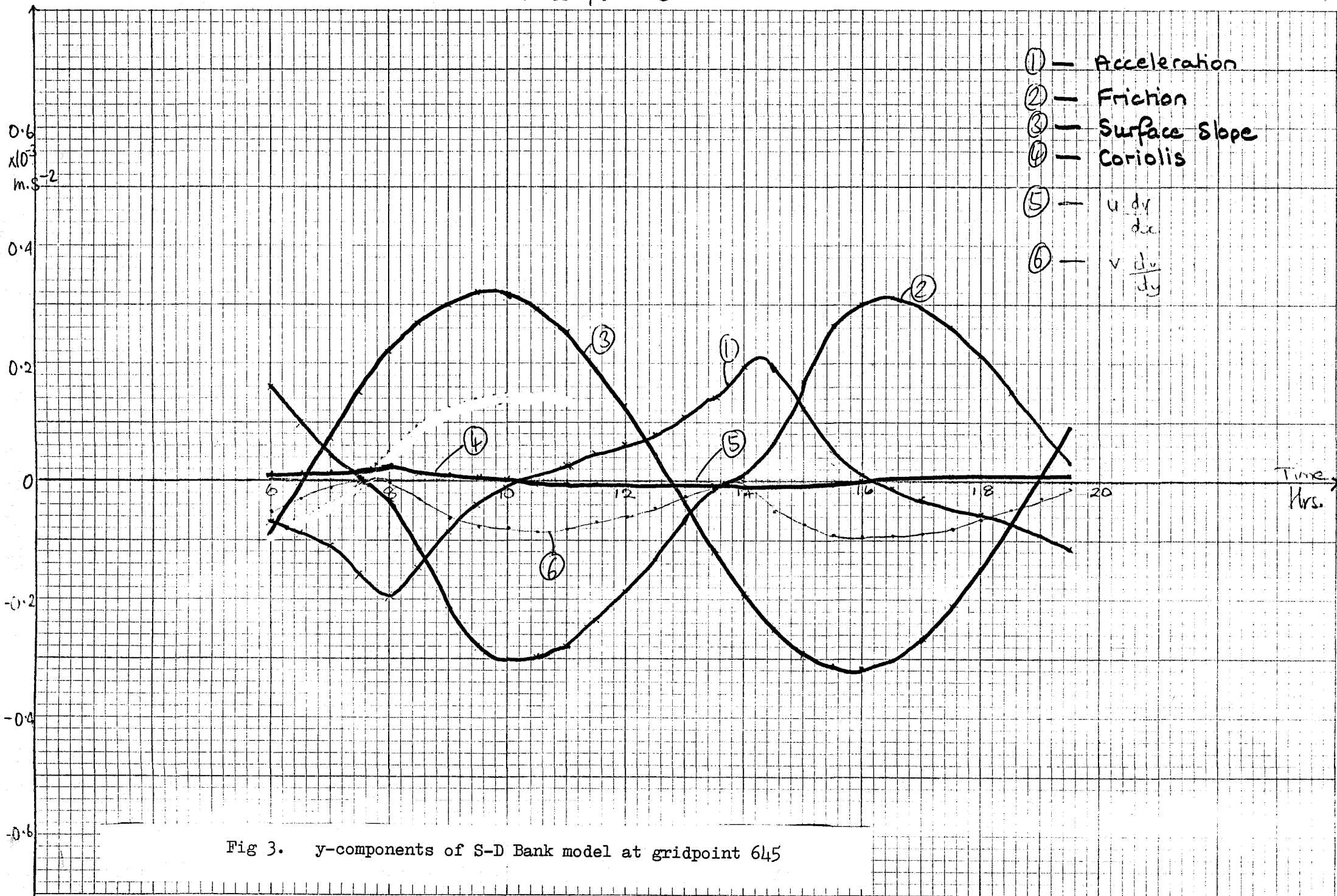Fig 2.   y-components of S-D Bank model at gridpoint 106

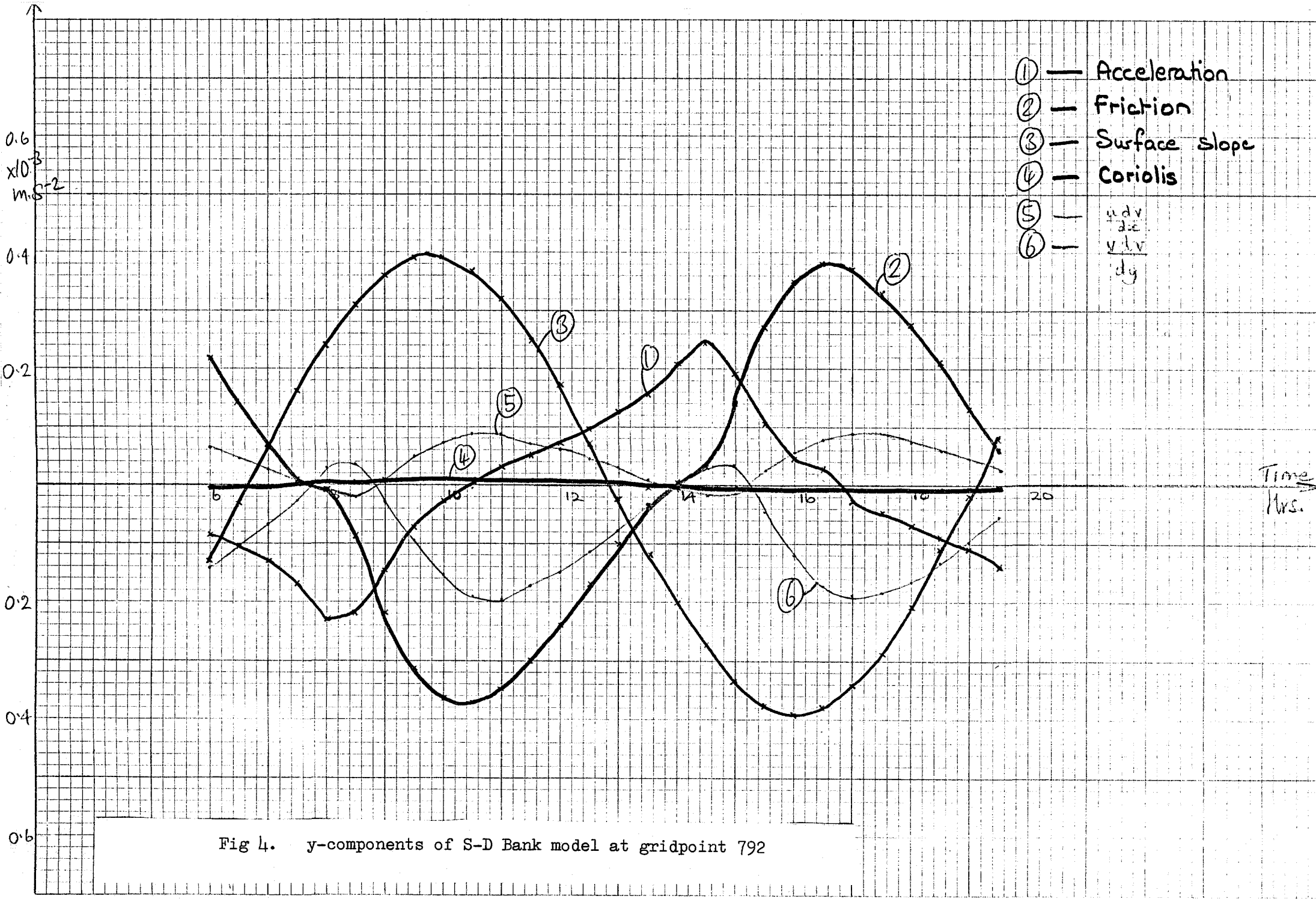Fig 3.   y-components of S-D Bank model at gridpoint 645

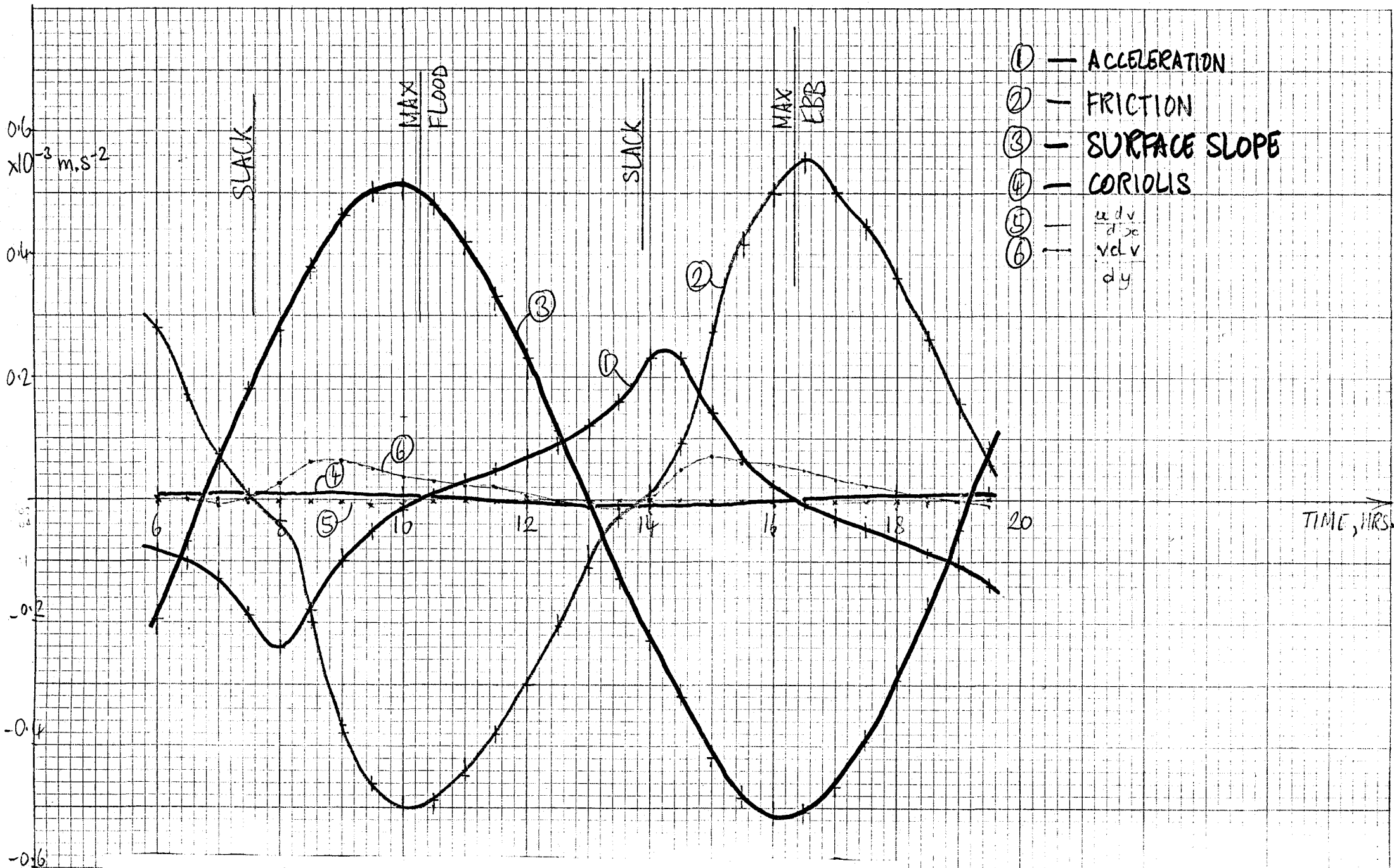Fig 4.   y-components of S-D Bank model at gridpoint 792

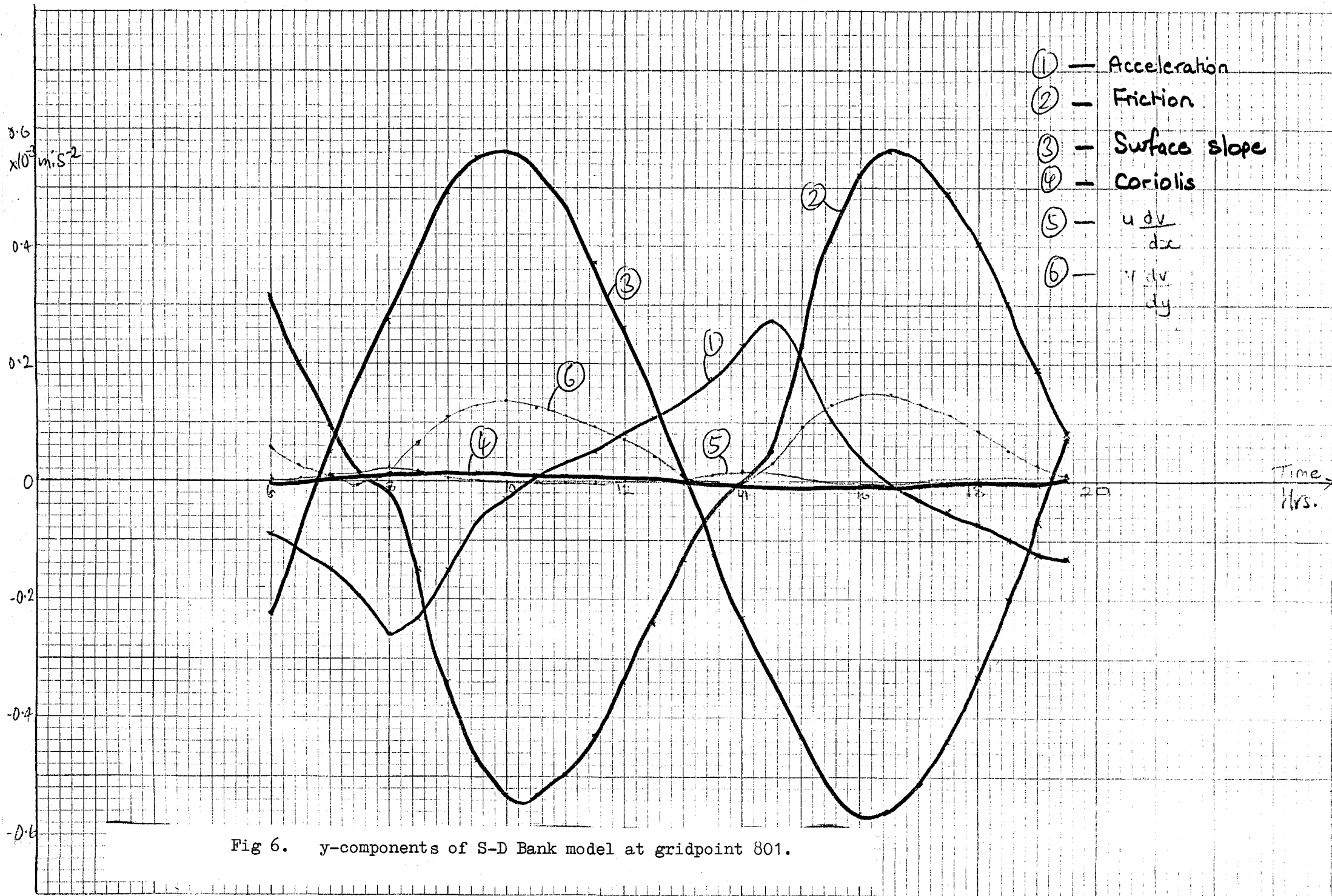Fig 5.   y-components of S-D Bank model at gridpoint 795

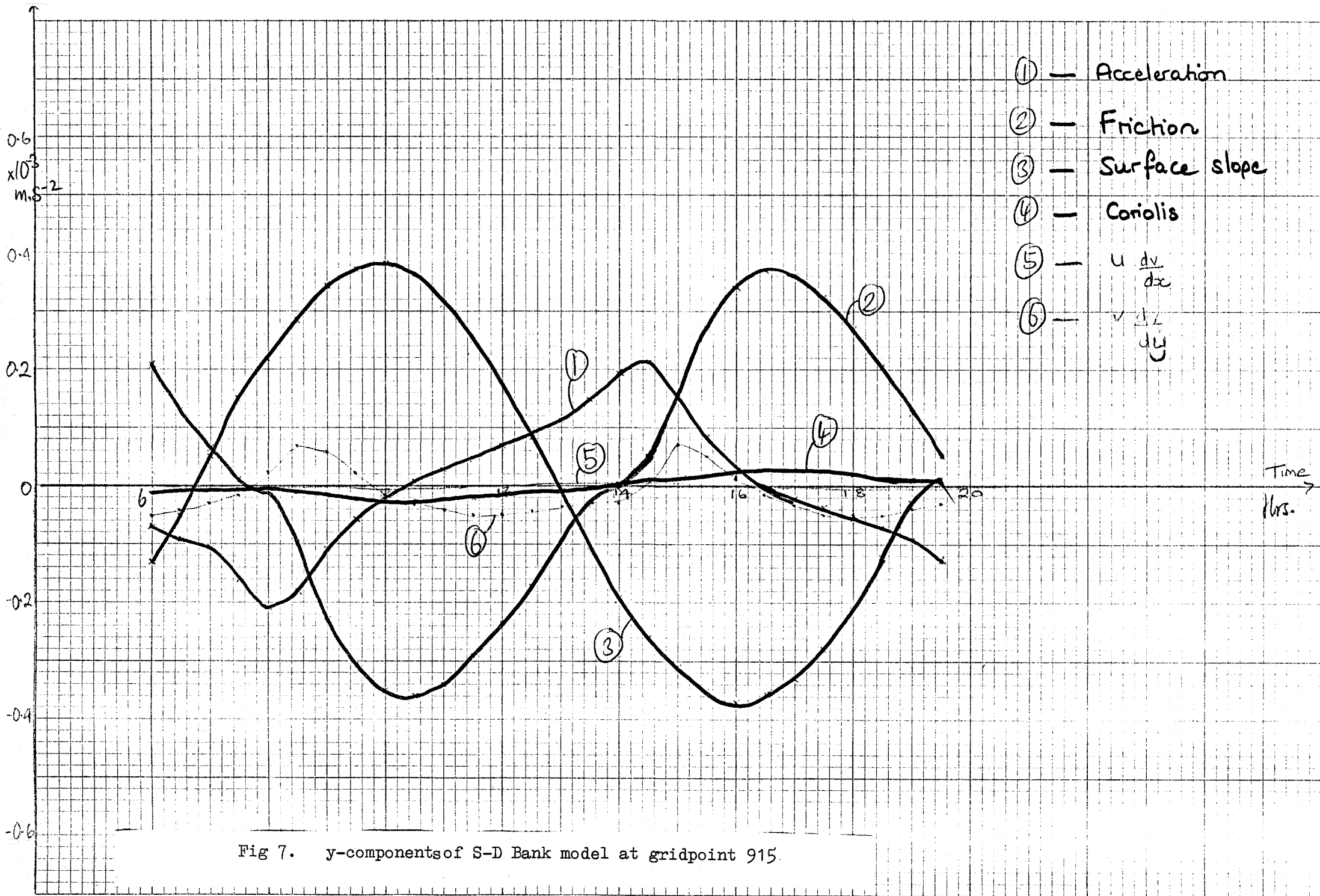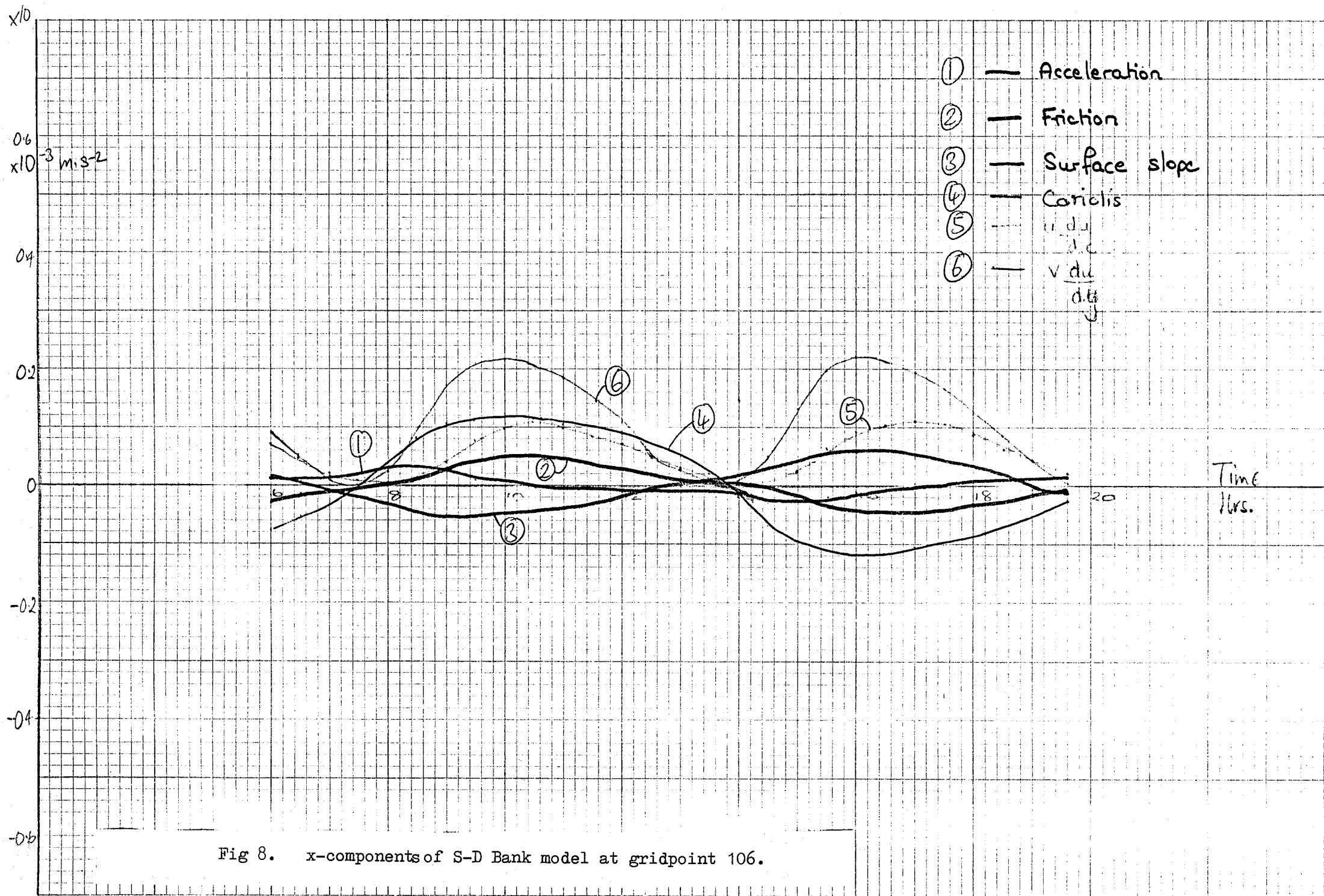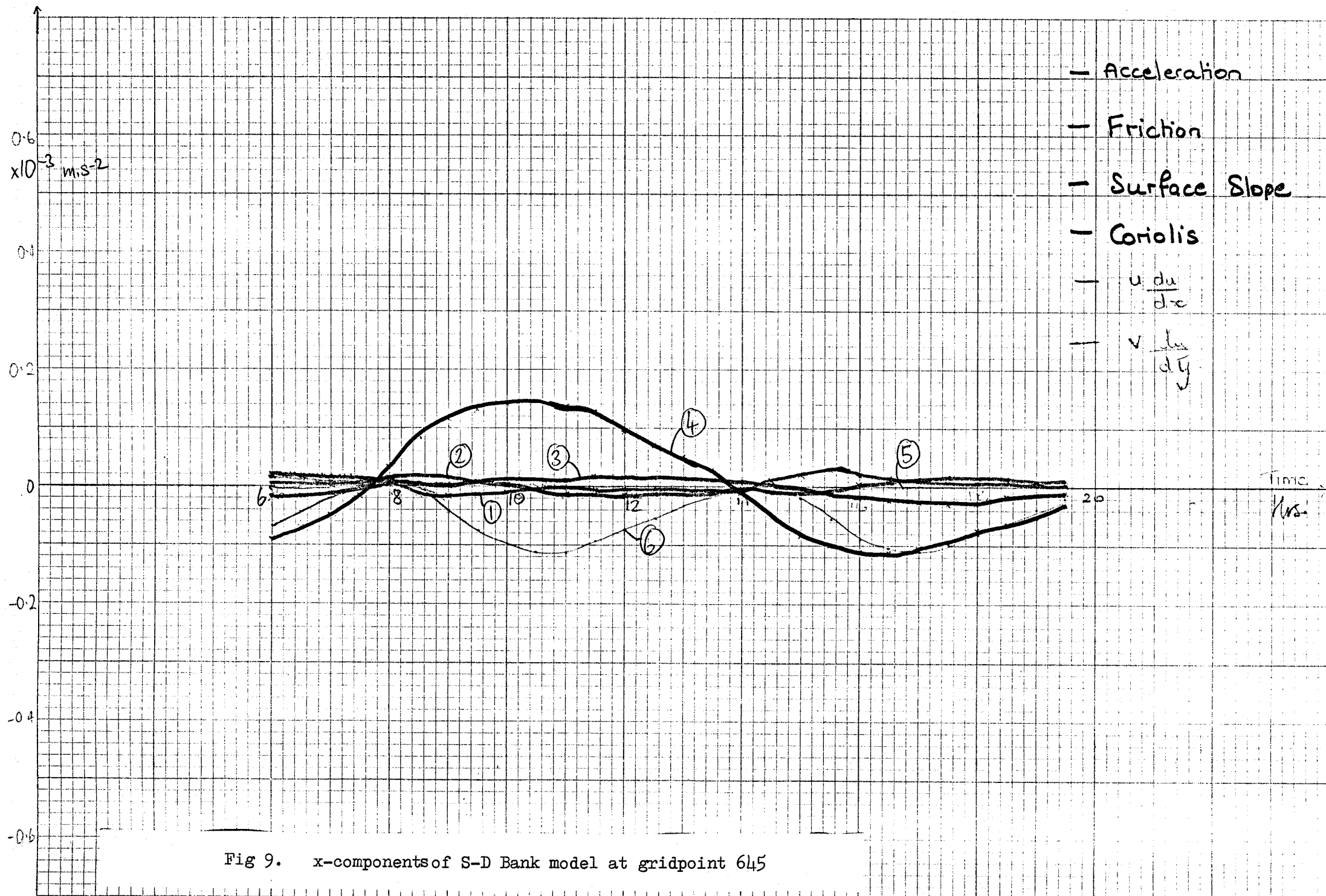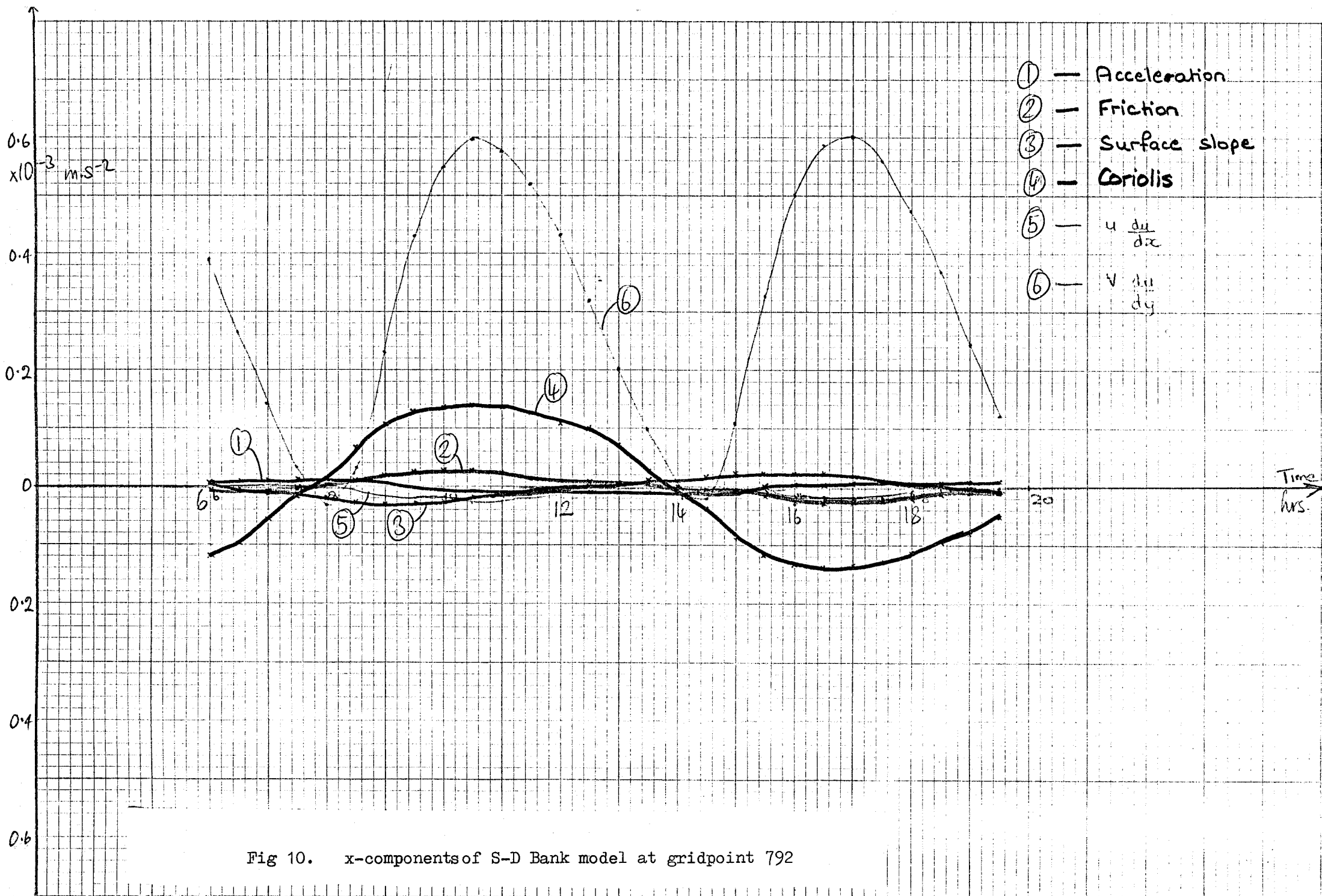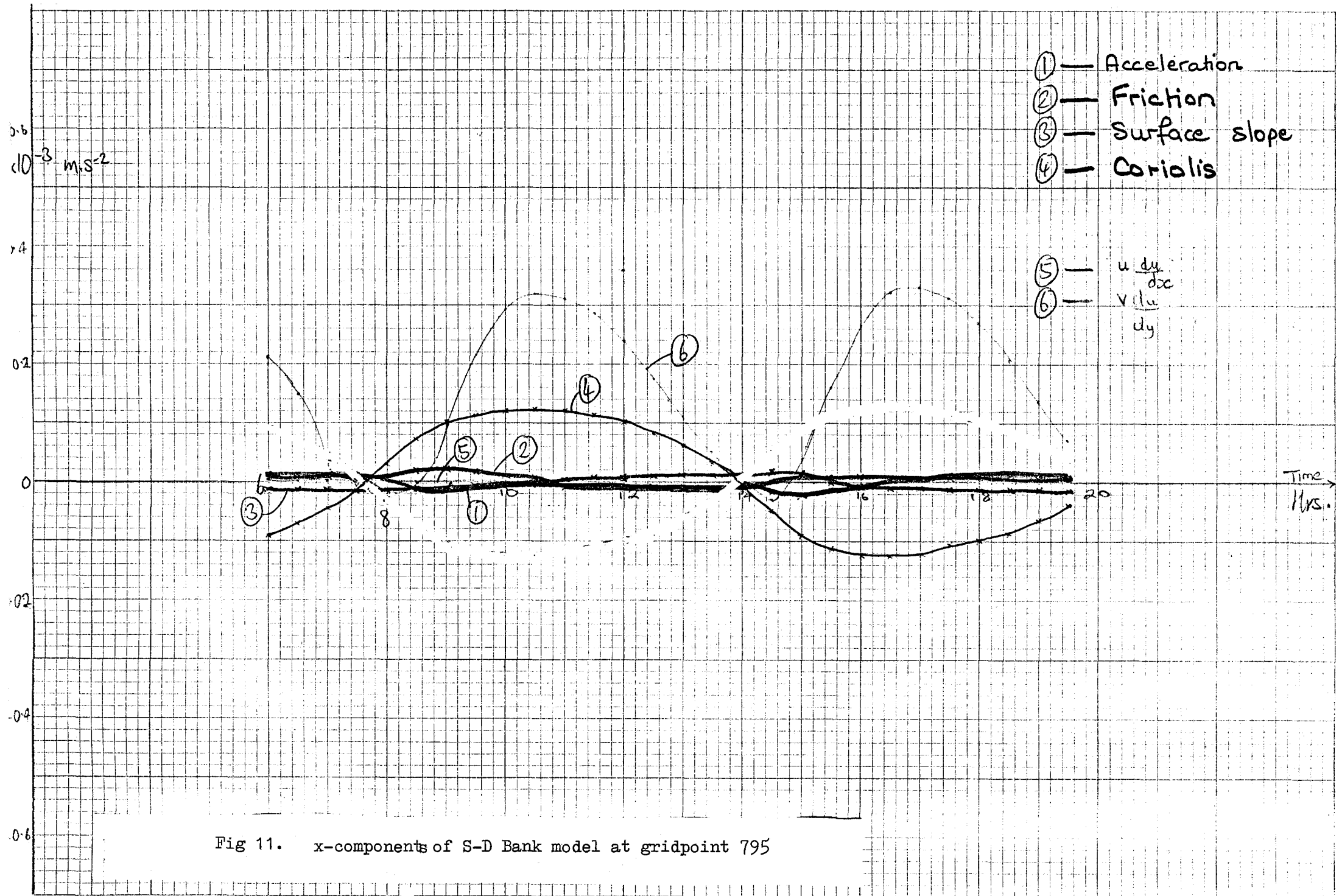Fig 6.   y-components of S-D Bank model at gridpoint 801.

Fig 7. y-components of S-D Bank model at gridpoint 915.

Fig 8.   x-components of S-D Bank model at gridpoint 106.

Fig 9.   x-components of S-D Bank model at gridpoint 645

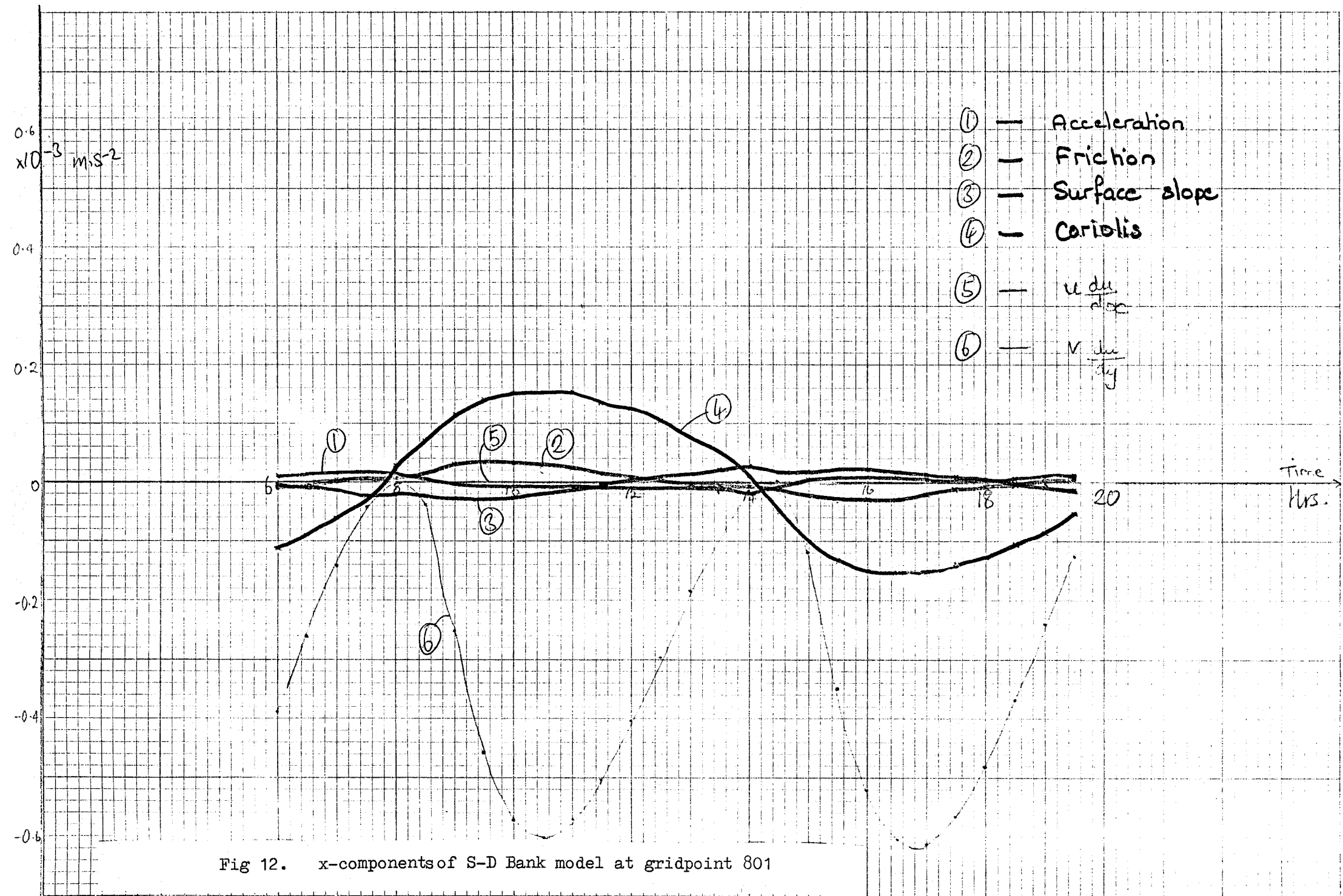Fig 10.   x-components of S-D Bank model at gridpoint 792

Fig 11.   x-components of S-D Bank model at gridpoint 795
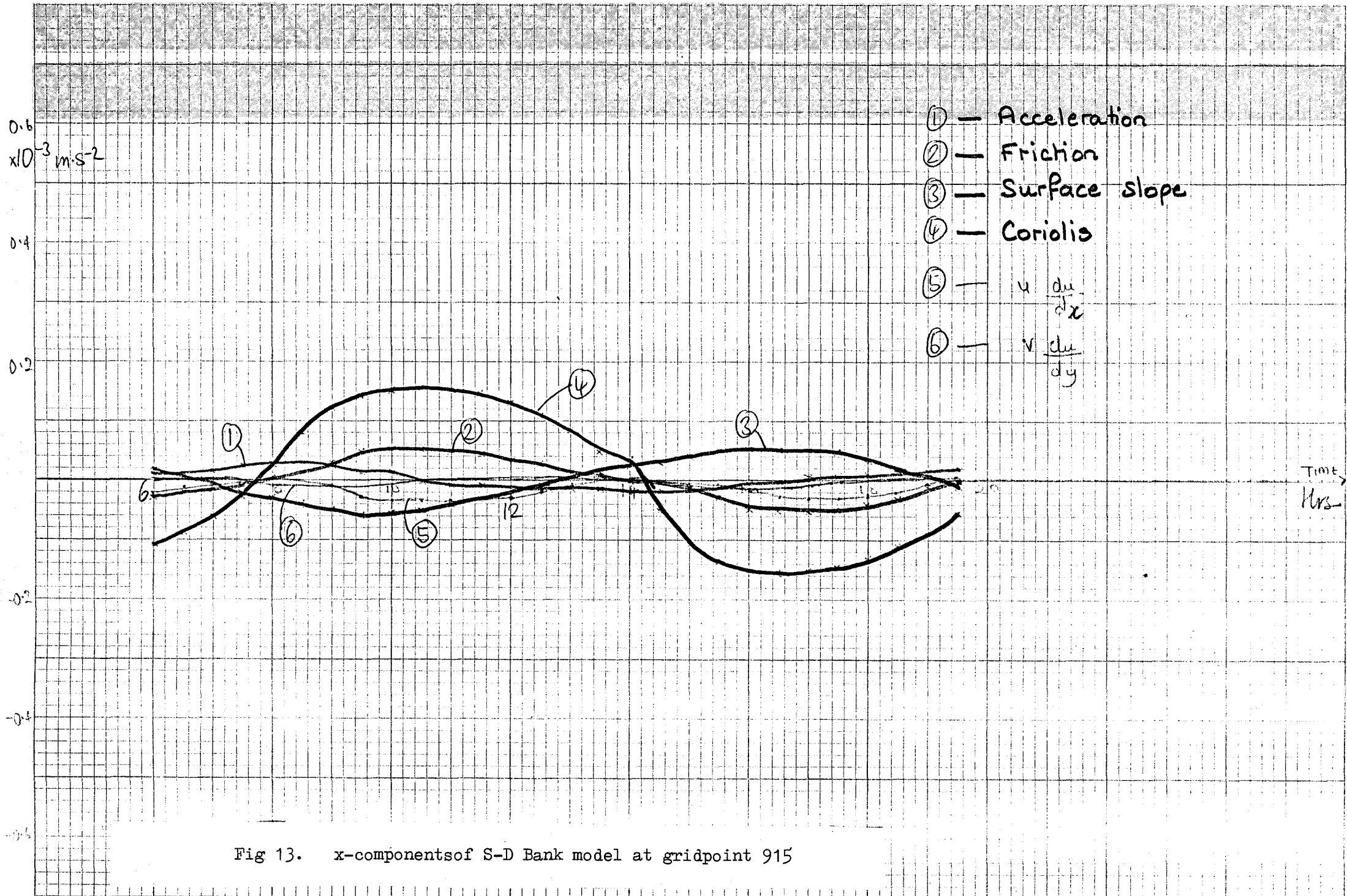
Fig 12.   x-components of S-D Bank model at gridpoint 801

Fig 13.   x-componentsof S-D Bank model at gridpoint 915